JGR Oceans

RESEARCH ARTICLE

10.1029/2023JC020387

Changes in Oceanic Radiocarbon and CFCs Since the 1990s

J. G. Lester[1], H. D. Graven[1], S. Khatiwala[2], and A. P. McNichol[3]

[1]Department of Physics, Imperial College London, London, UK, [2]Department of Earth Sciences, University of Oxford, Oxford, UK, [3]Department of Geology and Geophysics, NOSAMS, Woods Hole Oceanographic Institution, Woods Hole, MA, USA

Key Points:

- Recent trends in upper ocean $\Delta^{14}C$, pCFC-11, and pCFC-12 are negative, reflecting their decreasing atmospheric trends
- Increases in $\Delta^{14}C$ are only observed in a few places over 2000–2010s, showing oceanic bomb ^{14}C uptake has stopped and reversed
- Model-data $\Delta^{14}C$ and chlorofluorocarbon differences could be consistent with decadal ventilation changes and large-scale stratification or model errors

Supporting Information:

Supporting Information may be found in the online version of this article.

Correspondence to:

J. G. Lester,
j.lester16@imperial.ac.uk

Citation:

Lester, J. G., Graven, H. D., Khatiwala, S., & McNichol, A. P. (2024). Changes in oceanic radiocarbon and CFCs since the 1990s. *Journal of Geophysical Research: Oceans*, *129*, e2023JC020387. https://doi.org/10.1029/2023JC020387

Received 19 AUG 2023
Accepted 2 MAY 2024

Author Contributions:

Conceptualization: H. D. Graven
Data curation: J. G. Lester, H. D. Graven
Investigation: J. G. Lester, H. D. Graven
Methodology: J. G. Lester, H. D. Graven, S. Khatiwala
Resources: H. D. Graven, S. Khatiwala
Software: S. Khatiwala
Supervision: H. D. Graven, S. Khatiwala
Visualization: J. G. Lester
Writing – original draft: J. G. Lester
Writing – review & editing: J. G. Lester, H. D. Graven, S. Khatiwala, A. P. McNichol

Abstract Anthropogenic perturbations from fossil fuel burning, nuclear bomb testing, and chlorofluorocarbon (CFC) use have created useful transient tracers of ocean circulation. The atmospheric $^{14}C/C$ ratio ($\Delta^{14}C$) peaked in the early 1960s and has decreased now to pre-industrial levels, while atmospheric CFC-11 and CFC-12 concentrations peaked in the early 1990s and early 2000s, respectively, and have now decreased by 10%–20%. We present the first analysis of a decade of new observations (2007 to 2018–2019) and give a comprehensive overview of the changes in ocean $\Delta^{14}C$ and CFC concentration since the WOCE surveys in the 1990s. Surface ocean $\Delta^{14}C$ decreased at a nearly constant rate from the 1990–2010s (20‰/decade). In most of the surface ocean $\Delta^{14}C$ is higher than in atmospheric CO_2 while in the interior ocean, only a few places are found to have increases in $\Delta^{14}C$, indicating that globally, oceanic bomb ^{14}C uptake has stopped and reversed. Decreases in surface ocean CFC-11 started between the 1990 and 2000s, and CFC-12 between the 2000–2010s. Strong coherence in model biases of decadal changes in all tracers in the Southern Ocean suggest ventilation of Antarctic Intermediate Water was enhanced from the 1990 to the 2000s, whereas ventilation of Subantarctic Mode Water was enhanced from the 2000 to the 2010s. The decrease in surface tracers globally between the 2000 and 2010s is consistently stronger in observations than in models, indicating a reduction in vertical transport and mixing due to stratification.

Plain Language Summary The ocean contains many dissolved gases that can be measured by sampling ocean water from ships. Some of these dissolved gases are changing over time because their atmospheric concentrations are changing. By measuring these changes in the ocean, we can learn about ocean transport and mixing, which is an important factor regulating climate change. We describe ocean measurements from the past three decades of radiocarbon in dissolved inorganic carbon, that was affected by nuclear bomb testing, and of chlorofluorocarbon gases, CFCs, that were banned in the 1990s due to their destructive effects on the ozone layer. The measurements show how their oceanic distributions have changed, as a result of their atmospheric histories and the patterns of ocean uptake and transport. By comparing the measurements with ocean models, we can identify biases in the models that affect how well future climate change can be predicted. In the most recent decade, the presence of all three tracers is shown to be decreasing in the upper ocean, a reversal of the preceding decades. Also in the most recent decade, the decrease in surface tracers is stronger in the observations than the models, suggesting a change to upper ocean mixing and stratification.

1. Introduction

Ocean transient tracers have been integral to the development of our understanding of the dynamical processes and circulation of the ocean, and their role in the Earth's climate system and carbon cycle. One important tracer is radiocarbon (^{14}C), which is produced naturally in the atmosphere through cosmogenic radiation and mixes into the ocean through air-sea gas exchange, creating a unique distribution in the ocean interior as it decays over time (Key, 2001). The transient nature of ^{14}C arises from the nuclear weapons tests in the 1950 and 1960s that produced "bomb" ^{14}C in the atmosphere, almost doubling the natural background level (Manning et al., 1990). The mixing of bomb ^{14}C into the land and ocean carbon reservoirs, combined with the emission of CO_2 from the burning of fossil fuels, which are devoid of ^{14}C, has reduced the ratio $^{14}C/C$ in atmospheric CO_2 such that it is now the same as before the Industrial Revolution (Figure 1) (Graven et al., 2017, 2022). In the ocean, measured radiocarbon content is reported as $\Delta^{14}C$, the deviation of the ratio of $^{14}C/C$ atoms to a standard, corrected for age and fractionation effects (Stuiver & Polach, 1977).

Radiocarbon has been used to estimate the rates of gas exchange between the atmosphere and the ocean surface (Broecker & Peng, 1974), an approach which continues to be refined (Sweeney et al., 2007; Wanninkhof, 2014).

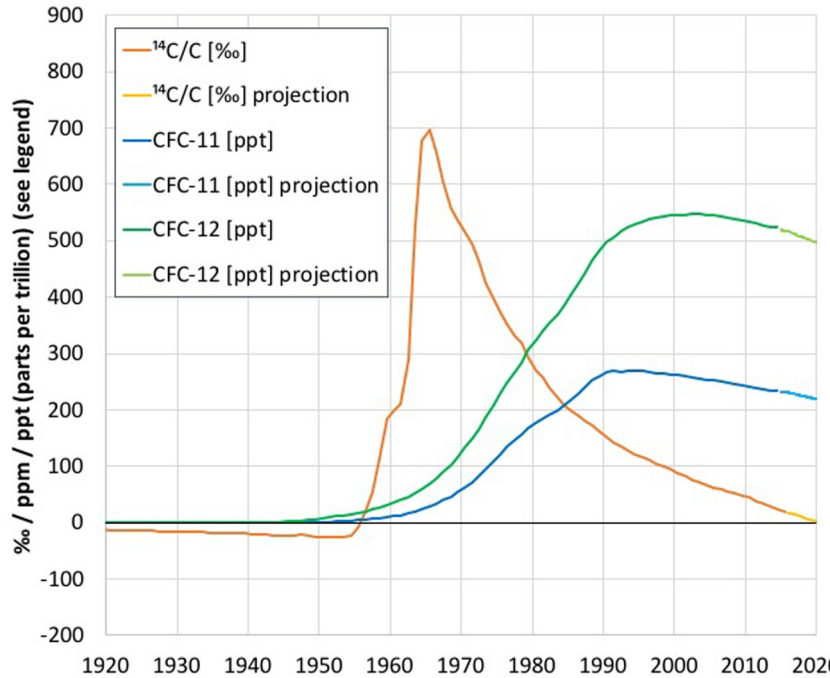

Figure 1. Trace gas atmospheric histories. Observed historical $\Delta^{14}C$ and CFC-11 and CFC-12 through 2015 (Bullister, 2015; Graven et al., 2017) and estimated $\Delta^{14}C$ and CFC-11 and CFC-12 for 2015–2020 (Graven, 2015; Meinshausen et al., 2020).

^{14}C has been used to understand the ventilation of the deep ocean (e.g., DeVries & Primeau, 2011; Holzer et al., 2010; Khatiwala et al., 2012; Toggweiler et al., 1989), water mass transformation (e.g., Müller et al., 2006), and the uptake of anthropogenic CO_2 by the ocean (Graven et al., 2012; Khatiwala et al., 2009).

Another important family of tracers are chlorofluorocarbons (CFCs): anthropogenic molecules composed of the elements chlorine, fluorine and carbon, first produced in the 1930s. Their manufacture was phased out in the 1990s after it was discovered they could destroy the ozone layer (Molina & Rowland, 1974). CFCs have been absorbed by the surface ocean through air-sea gas exchange, and are mixing into the ocean interior. The measured concentration of CFCs in seawater can therefore be used to help understand ocean ventilation, mixing and transport pathways (Fine, 2011). The most commonly measured CFCs are CFC-11 and CFC-12, which peaked in atmospheric concentration in the 1990 and 2000s, respectively, according to their different sources and atmospheric lifetimes (Figure 1).

Oceanic CFCs have been used to identify deep western boundary currents (Smethie et al., 2000; Weiss et al., 1985); observe ocean ventilation and estimate subduction and formation rates (Purkey et al., 2018; Wallace & Lazier, 1988); and estimate the anthropogenic CO_2 in the ocean, in concert with other ocean tracers (Khatiwala et al., 2009; Sabine et al., 2004; Tanhua et al., 2009). CFC measurements from hydrographic transects conducted in different decades have been used to identify changes in ocean circulation (Tanhua et al., 2013; Ting & Holzer, 2017; Waugh et al., 2013).

Ship-based observations are the only way to measure oceanic $\Delta^{14}C$ and CFCs. Global ocean hydrographic survey campaigns were initiated in the 1970s with the GEOSECS program (Craig, 1972, 1974; Craig & Turekian, 1976, 1980). The WOCE and CLIVAR global programs followed in the 1990 and 2000s (Chapman, 1998; Trenberth, 1999), and now the international GO-SHIP consortium coordinates seagoing efforts from the 2010s forward (Talley et al., 2016). Repeated surveys of meridional and zonal ocean sections allow for comparisons in time. While studies of decadal changes have been made in the past (e.g., Fine, 2011; Graven et al., 2012; Key, 2001; Waugh et al., 2013), there are now sections which have been occupied two or more times, allowing longer term trends and variability to be investigated.

In this work we look at $\Delta^{14}C$ and CFCs together, because over the time period we consider they can be considered conservative tracers of oceanic transport and mixing, but they also differ in many ways. For instance, the

atmosphere-surface ocean equilibration time for CFCs is ∼1 month but it is ∼10 years for $\Delta^{14}C$ (Broecker & Peng, 1974). The temperature dependence of CFC solubility differs markedly from that of ^{14}C, so air-sea exchange imprints different meridional trends on the two classes of tracer. The performance of ocean models can vary between tracers due to the differences in air-sea exchange and in the timescales that encompass different aspects of ocean circulation (e.g., Matsumoto et al., 2004).

Here we present a global compilation of oceanic $\Delta^{14}C$ and CFC-11 and CFC-12 observations since the global WOCE survey in the 1990s. We identify the changes in each tracer and their spatial distribution between each decade. We compare the observed decadal changes in each tracer to those modeled by two state-of-the-art ocean models. By comparing the tracer observations and models, we identify either possible regions of decadal ocean circulation variability, or poor model performance, and compare to prior studies.

2. Methods

2.1. Ocean Observations

We use observations of $\Delta^{14}C$ in dissolved inorganic carbon (DIC) and the partial pressure of CFC-11 and CFC-12 (pCFC-11 and pCFC-12) from the GLODAPv2.2019 database (Key et al., 2015; Olsen et al., 2016, 2019) (Table S1 in Supporting Information S1). We also use additional data not included in GLODAPv2.2019, summarized in Table S2 in Supporting Information S1 (Barbero et al., 2018; Baringer et al., 2016; Curry, 2012; Druffel, 2016; King, 2018; Macdonald, 2016; Macdonald & Briggs, 2018; McCartney, 2012; Mecking & Rosso, 2018; Orsi & Rosso, 2020; Perkin, 1999; Rintoul, 2018; Speer & Schulze, 2018; Uchida et al., 2011; Volkov & Menezes, 2018). $\Delta^{14}C$ and pCFC samples meeting the WOCE data quality flag 2 "acceptable" standard (Olsen et al., 2016) and which had valid accompanying potential density anomaly (σ_θ) measurements were selected. The measurement uncertainty on the $\Delta^{14}C$ observations we present is typically 2‰–3‰ and the measurement uncertainty on the pCFC observations is ∼2 ppt. We focus on recent measurements since the 1980s but also consider some early measurements including pre-GEOSECS data compiled by Graven et al. (2012) and estimates of "natural" radiocarbon from GLODAP (Key et al., 2004; Rubin & Key, 2002).

We examine decadal changes in the tracers along more than 20 hydrographic sections in observations from 1987 to 2019 (Table S1 in Supporting Information S1 and Figure 2). In order to compare the sometimes sparsely sampled tracer data between different time periods, following Graven et al. (2012) we bin the data by depth or potential density anomaly (σ_θ) and latitude/longitude, calculating an average tracer value for each bin per time period from which we then subtract the earlier time period to calculate the change, Δ, in tracer (e.g., $\Delta\Delta^{14}C$). Generally, each section has enough samples to allow a reasonable comparison.

We show comparisons in depth coordinates in the main text and comparisons using potential density anomaly coordinates in Supporting Information S1 (Figure S1–S3). Comparisons along potential density anomaly coordinates help to remove the effect of vertical displacement of water masses by isopycnal heave. The observations are presented in decadal clusters for the 1990, 2000, and 2010s, to allow comparison across oceans basins with time. Some transects from the late 1980s in the Atlantic and Indian Oceans have also been considered because there are limited measurements there in the 1990s. The tracer changes are reported per 10 years, normalizing for the number of years separating the observations.

In general the ΔpCFC-11 profiles are less scattered than the $\Delta\Delta^{14}C$ profiles, because the data has been recorded at a much higher horizontal and vertical resolution, and the absence of CFCs in the ocean interior removes scatter in the deeper waters. However, we have also excluded numerous CFC sections from this work because they showed inconsistencies (Figures S4 and S5 in Supporting Information S1), as described in Table S3 in Supporting Information S1. The sections we have excluded (Table S3 in Supporting Information S1) reflect that in some regions, pCFC measurement errors or instrument offsets are larger than those reported. Some sections are not consistent with neighboring sections, despite corrections made in GLODAPv2.2019.

2.2. Ocean Modeling

We compare the observations with $\Delta^{14}C$ and CFC simulations from two different ocean general circulation models (Table S4 in Supporting Information S1). In both models $\Delta^{14}C$ is simulated using the "abiotic" formulation used in the Ocean Model Intercomparison Project (OMIP; Orr, Najjar, et al., 1999; Orr et al., 2017). CFCs are modeled using the equivalent protocols for CFCs (Orr, Dutay, et al., 1999; Orr et al., 2017). Atmospheric

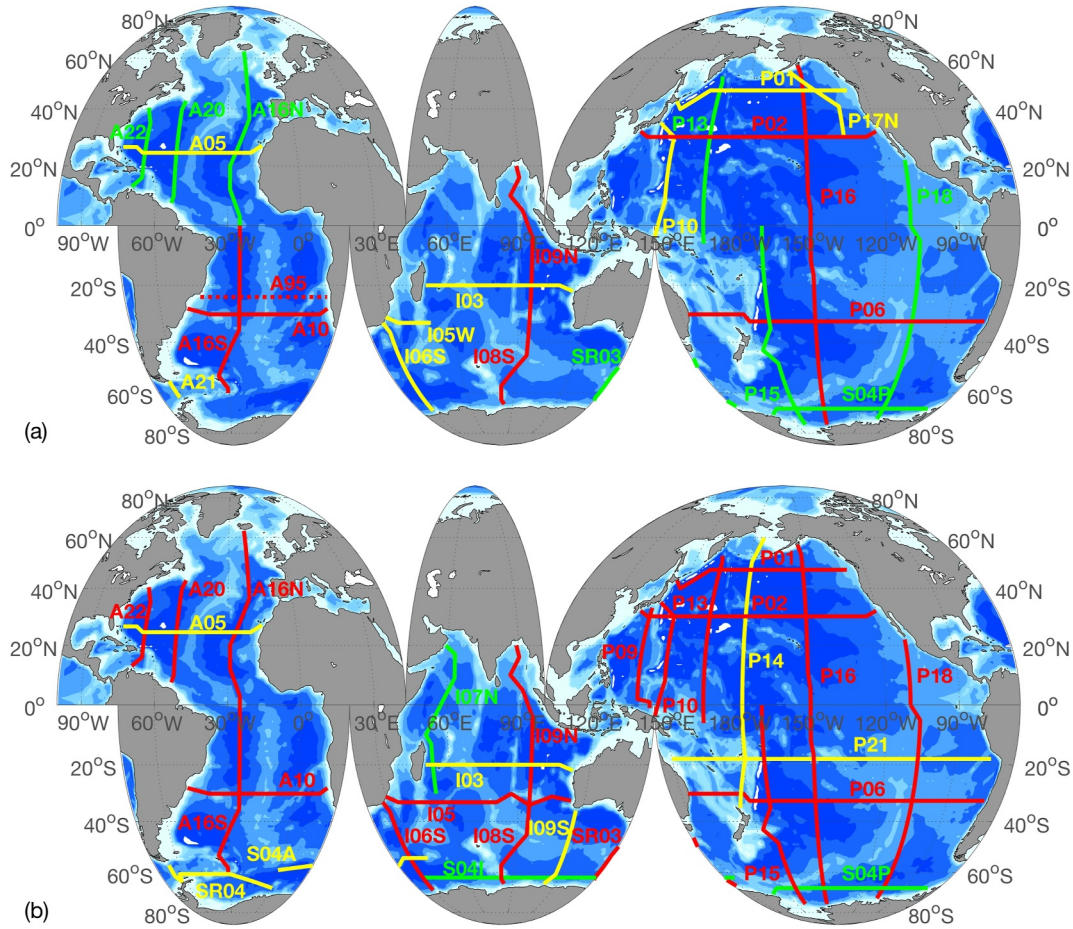

Figure 2. Geographical overview of (a) $\Delta^{14}C$ and (b) CFC sections used in this study, where yellow lines were occupied in the 1990 and 2000s, green lines in the 1990 and 2010s, and red lines were occupied in all three decadal clusters. See Table S3 in Supporting Information S1 for sections excluded from detailed analysis in this study.

composition for 1850 to 2015 was specified by Meinshausen et al. (2017) and Graven et al. (2017), which both account for zonal differences in composition.

First, we simulated $\Delta^{14}C$ and CFC using state estimates from Estimating the Climate and Circulation of the Ocean version 4 (ECCOv4; Forget et al., 2015) based on a global configuration of the MITgcm (Marshall et al., 1997) model with a horizontal resolution of ~0.8° × ~0.5°, and 50 depth levels. ECCOv4 uses an adjoint strategy (Wunsch & Heimbach, 2007) to minimize the misfit between the model and a range of hydrographic properties, including profiled potential temperature and salinity, and gridded products for sea surface temperature, sea surface salinity, sea level anomaly and mean dynamic topography between 1992 and 2011 (Forget et al., 2015). We use a climatological average of the circulation over this period encapsulated as monthly-mean transport matrices (TMs) and use the transport matrix method (Khatiwala, 2007, 2018; Khatiwala et al., 2005) to simulate CFC-11, CFC-12 and abiotic DIC and ^{14}C in DIC "off-line" (Khatiwala et al., 2018). For gas exchange velocity, a quadratic function of the local wind speed (Wanninkhof, 1992) was used with 6-hourly climatological Common Ocean-ice Reference Experiments—Corrected Normal Year Forcing (CORE-CNYF; Large & Yeager, 2009). A gas transfer coefficient of 0.272 (cm/hr) (s^2/m^2) was selected such that when combined with the CORE forcing the global mean gas exchange velocity was approximately 17 cm/hr, in line with recent studies (Khatiwala et al., 2018; Naegler, 2009). Abiotic DIC and ^{14}C in DIC were spun up to a steady state over 5,000 years, using constant pre-industrial forcing of 277.89 ppm for CO_2 and 0‰ for $\Delta^{14}C$. The historical simulation began to vary atmospheric CO_2 concentration in 1765, following Meinshausen et al. (2017), while atmospheric $\Delta^{14}C$ remained at 0‰ until 1850. The simulation was continued after 2015 until 2019 using the RCP 8.5 forcing for atmospheric

CO_2 (van Vuuren et al., 2011) and $\Delta^{14}C$ (Graven, 2015), and the SSP1-2.6 projection for CFC-11 and CFC-12 (Meinshausen et al., 2020).

Second, we use output from the "historical" run of the Community Earth System Model Version 2 (CESM2; Danabasoglu et al., 2020) for the Coupled Model Intercomparison Project-Phase 6 (CMIP6; Eyring et al., 2016). CESM2 is a fully coupled earth system model with interactive ocean, atmosphere, ice, land and ocean biogeochemical components. CESM2 uses the Parallel Ocean Program ocean model with a horizontal resolution of $1.125° \times 0.5°$ and 60 depth levels (Smith et al., 2010). Abiotic DIC and ^{14}C in DIC were implemented following Orr et al. (2017) and spun up using a Newton-Krylov-based solver (Khatiwala, 2008; Li & Primeau, 2008; Lindsay, 2017) with a constant pre-industrial atmospheric CO_2 concentration of 284.7 ppm and $\Delta^{14}C$ of 0‰. The historical simulation with varying CO_2, $\Delta^{14}C$, CFC-11, and CFC-12 begins in 1850 (Graven et al., 2017; Meinshausen et al., 2017). CESM2 used a gas transfer coefficient of 0.251 (cm/hr) (s^2/m^2) (Wanninkhof, 2014), which would equate to an average gas exchange velocity of 15.7 cm/hr were the CORE forcing used. Modeled monthly ocean CFC-11 and CFC-12 concentrations were converted to equilibrium partial pressures pCFC-11 and pCFC-12 by dividing by their respective solubility functions (Doney & Bullister, 1992; Warner & Weiss, 1985). All model output was averaged from monthly into annual means. The annual mean model output was then interpolated to the location of each observation in each year and binned in the same way as the observations.

The ocean models we present simulations from are the next generation to those used in Graven et al. (2012). Improvements made to CESM2 from its preceding version, CCSM, include increased mesoscale eddy diffusivities at depth in the ocean, and a new wave model component coupled with a new Langmuir mixing parameterization (Danabasoglu et al., 2020). Improvements from ECCO to ECCOv4 are provided by Argo floats enhancing the data coverage of previously poorly sampled regions like the Southern Ocean (Forget et al., 2015).

3. Results

First, to illustrate the expected tracer changes in the ocean since the 1950s and over the 1990–2010s period we will focus on, we present simulated vertical profiles of global average $\Delta^{14}C$, pCFC-11, and pCFC-12 from the ECCOv4-TM model (Figure 3). The patterns reflect the oceanic propagation of a tracer increasing and then decreasing in the atmosphere, with differences between the tracers related to the timing and shape of the atmospheric variations (Figure 1).

In 1950, while the simulated oceanic pCFC-11 and pCFC-12 concentrations were nearly zero, natural radiocarbon was present and global average $\Delta^{14}C$ decreased exponentially with depth from −60‰ at the surface to almost −200‰ below 2,000 m (Figure 3), as previously found by others (Graven et al., 2012; Khatiwala et al., 2018). All tracers increase from the 1950–1960s, and 1960–1970s, with the largest changes in the surface ocean (Figure 3). From the 1970–1980s the depth of the maximum increase in $\Delta^{14}C$ drops from the surface to several hundred meters depth. From the 1980 to the 1990s, global average $\Delta^{14}C$ starts to decrease above 200 m, while continuing to increase below 200 m. The depth of this sign change deepens from the 1990–2000s, and then the 2000–2010s, with the increases in $\Delta^{14}C$ becoming weaker over time. A nearly linear trend of −20‰ per decade is simulated in global average surface ocean $\Delta^{14}C$ since the 1980s. Atmospheric $\Delta^{14}C$ exhibited a nearly linear trend of larger magnitude, −50‰/decade, since the 1990s (Figure 1; Graven et al., 2017).

For pCFC-11, increases that are strongest in the surface ocean continue until a subsurface maximum in pCFC-11 change emerges between the 1990–2000s, after atmospheric CFC-11 peaked (Figure 1). Then from the 2000–2010s there is a decrease in pCFC-11 above 200 m and a weaker increase from 200 to 1,000 m, similar to the pattern for $\Delta^{14}C$. pCFC-12 lags these patterns by roughly 10 years, with negative changes only appearing in surface pCFC-12 for the 2000–2010s.

In observations from recent decades, we thus expect to see weakening increases in tracer concentration, with decreases appearing at the surface and the depth of the sign change lowering over time. Some of these changes have been reported previously (Fine et al., 2017; Graven et al., 2012; Key, 2001; Khatiwala et al., 2018). Here we take a unique, global and multidecadal view on the observed changes of the three tracers and how they compare with models.

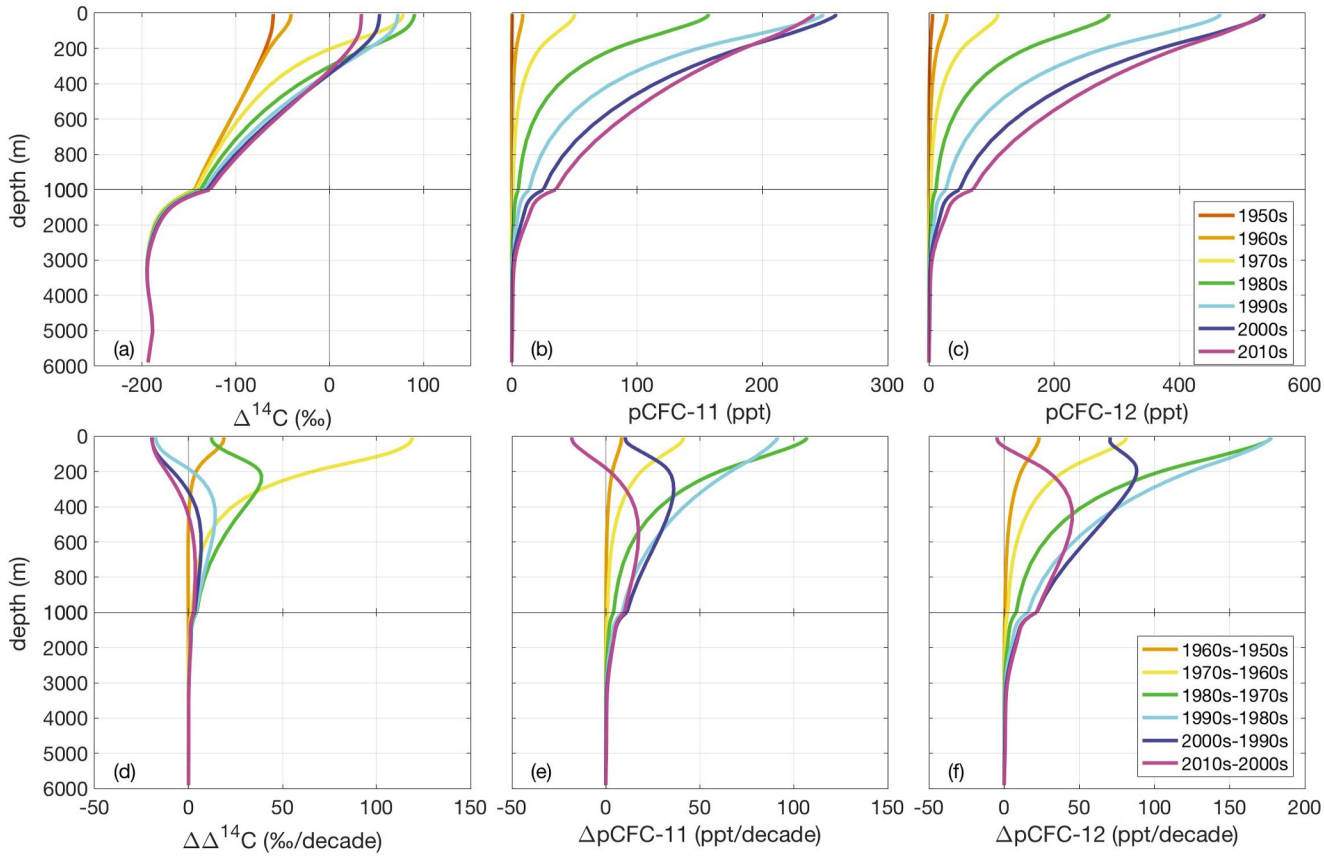

Figure 3. Simulated global decadal average depth profiles of (a) $\Delta^{14}C$, (b) pCFC-11, (c) pCFC-12, (d) $\Delta\Delta^{14}C$ decadal difference (more recent decade minus earlier decade), (e) ΔpCFC-11 decadal difference and (f) ΔpCFC-12 decadal difference in the ECCOv4-TM model.

3.1. Observed Large Scale Decadal Tracer Changes

In this section, we provide an overview of the oceanic observations collected over the last three decades. First, we examine the observed sea-air gradients in $\Delta^{14}C$. Based on coral records, early oceanic measurements and reconstructions, prior to 1957 the sea-air $\Delta^{14}C$ gradient was consistently negative, at around −50‰ in the mid- and low-latitudes, while upwelling and mixing of ^{14}C depleted water reduced $\Delta^{14}C$ sea-air gradients to around −100‰ in the Southern Ocean (Figure 4) (Key et al., 2004; Rubin & Key, 2002). Bomb ^{14}C greatly enhanced the negative $\Delta^{14}C$ sea-air gradient observed in the 1970s, driving strong uptake of ^{14}C by the global ocean (Broecker & Peng, 1974). As ^{14}C accumulated in the shallow ocean and atmospheric $\Delta^{14}C$ declined through the 1980–2000s, sea-air gradients reduced with time, as did horizontal gradients in the ocean (Figure 4) (Graven et al., 2012). Now, the observations from the first half of the 2010s show there is a positive sea-air gradient everywhere but the Southern Ocean south of 40°S and the North Pacific Ocean north of 40°N, indicating that most ocean areas are now outgassing ^{14}C (Figure 4). We also note that the subtropical peaks in $\Delta^{14}C$ caused by accumulation of ^{14}C in the subtropical gyres are absent in the 2010s, and average $\Delta^{14}C$ is nearly constant between 30°S and 30°N. Horizontal $\Delta^{14}C$ gradients in the ocean between 30°S and 30°N in the pre-bomb era were also very small, but the mean level in the 2000s was approximately +40‰ instead of −50‰.

In order to present the data from the many seagoing observational campaigns, we show measurements of $\Delta^{14}C$, pCFC-11, and pCFC-12 from hydrographic transects in the 1990s compiled on one figure, and we show the decadal changes in each tracer from repeat measurements of hydrographic sections in the 2000 and 2010s (see Figures 5–7).

In the 1990s (Figure 5a), as described in Key et al. (2004), $\Delta^{14}C$ is highest across the surface ocean, with high $\Delta^{14}C$ extending downward in the centers of the downwelling subtropical gyres and in the North Atlantic deep water (NADW). In the Southern Ocean, ventilated mode and intermediate water carry high $\Delta^{14}C$ into the ocean

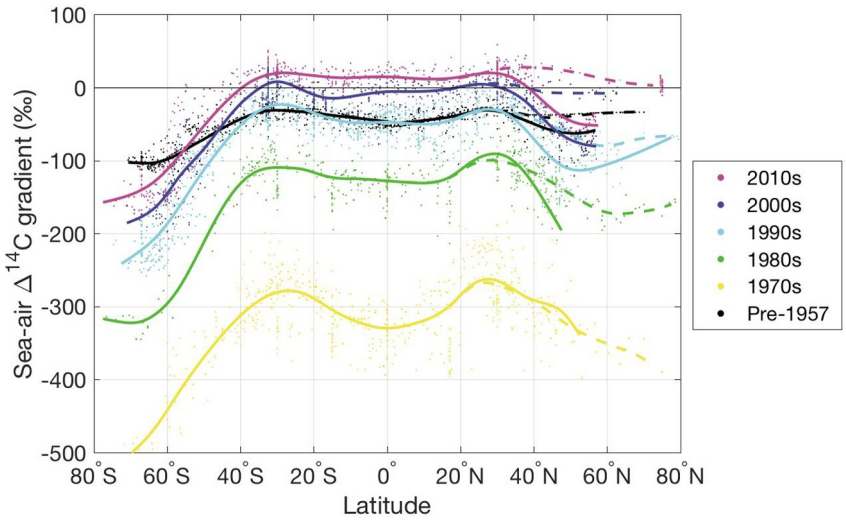

Figure 4. Surface ocean $\Delta^{14}C$ with the decadal atmospheric mean for each decade subtracted. "Pre-1957" measurements include calculated "natural" radiocarbon from GLODAP (Key et al., 2004; Rubin & Key, 2002). Solid lines are for all data and the North Pacific north of 30°N, and dashed lines are for all data and the North Atlantic north of 30°N. Lines are smoothed splines.

interior north of the Antarctic Circumpolar Current. Upwelling south of 60°S in the Southern Ocean draws low $\Delta^{14}C$ water to the surface. The lowest $\Delta^{14}C$ is found in the Pacific north of 40°N around 2,500 m depth, corresponding to the most aged ocean waters, and the North Pacific Subpolar Gyre upwells low $\Delta^{14}C$ toward the surface.

From the 1990s through to the 2010s, surface $\Delta^{14}C$ decreases everywhere (Figures 5b and 5c). The rate of surface decrease is around −20‰/decade in each time period, consistent with predicted changes (Figure 3d). From the 1990 to the 2000s, strong (<20‰/decade) increases in $\Delta^{14}C$ are found deeper down, at depths of 400–1,000 m, notably in the zonal sections around 30°S in each basin (Figure 5b). From the 2000 to the 2010s, areas of increasing $\Delta^{14}C$ are much smaller and less coherent. Only the eastern North Indian Ocean at 500–1,500 m and the western South Atlantic Ocean at 1,500–3,000 m show consistent increases (Figure 5c). Sampling density for $\Delta^{14}C$ is much lower in the 2000 and 2010s, so some areas with increases in $\Delta^{14}C$ may have been missed by the observations.

For CFCs, the highest pCFCs are found across the surface ocean in the 1990s, while the majority of the ocean interior remains devoid of CFCs (Figures 6a and 7a). High pCFC extends deepest in the centers of the downwelling subtropical gyres, in mode and intermediate waters and in NADW, similar to $\Delta^{14}C$. The ventilation of Antarctic Bottom Water (AABW) is much clearer via CFCs than $\Delta^{14}C$ due to greater spatial coverage and the absence of a natural pCFC distribution (Figures 6a and 7a).

From the 1990 to the 2000s, observed pCFC-11 begins to decrease across the surface ocean (except in the South Atlantic and South Indian Ocean due to earlier measurement dates in the 1980s instead of 1990s, see Table S1 in Supporting Information S1), while continuing to increase into the deeper ocean (Figure 6b). The large-scale near-surface decrease in pCFC-11 is observed earlier than predicted by ECCOv4-TM, where a small increase was simulated in the global average surface pCFC-11 between 1990 and 2000s (Figure 3e). pCFC-12 increases at the surface between the 1990 and 2000s both in observations (Figure 7b) and in the model (Figure 3f). From the 2000 to the 2010s, observed tracer changes are negative for both CFCs in the upper 200 m of the ocean. Further analysis of observed tracer changes in different ocean basins and their comparison with ocean models is given in Section 3.3 below.

3.2. Large-Scale Model Biases

Here we compare the observations to large scale patterns in both the ECCOv4-TM and CESM2 simulations in each decade. First, we compare surface observations of $\Delta^{14}C$ with the models (Figure 8 and Figures S6 and S7 in

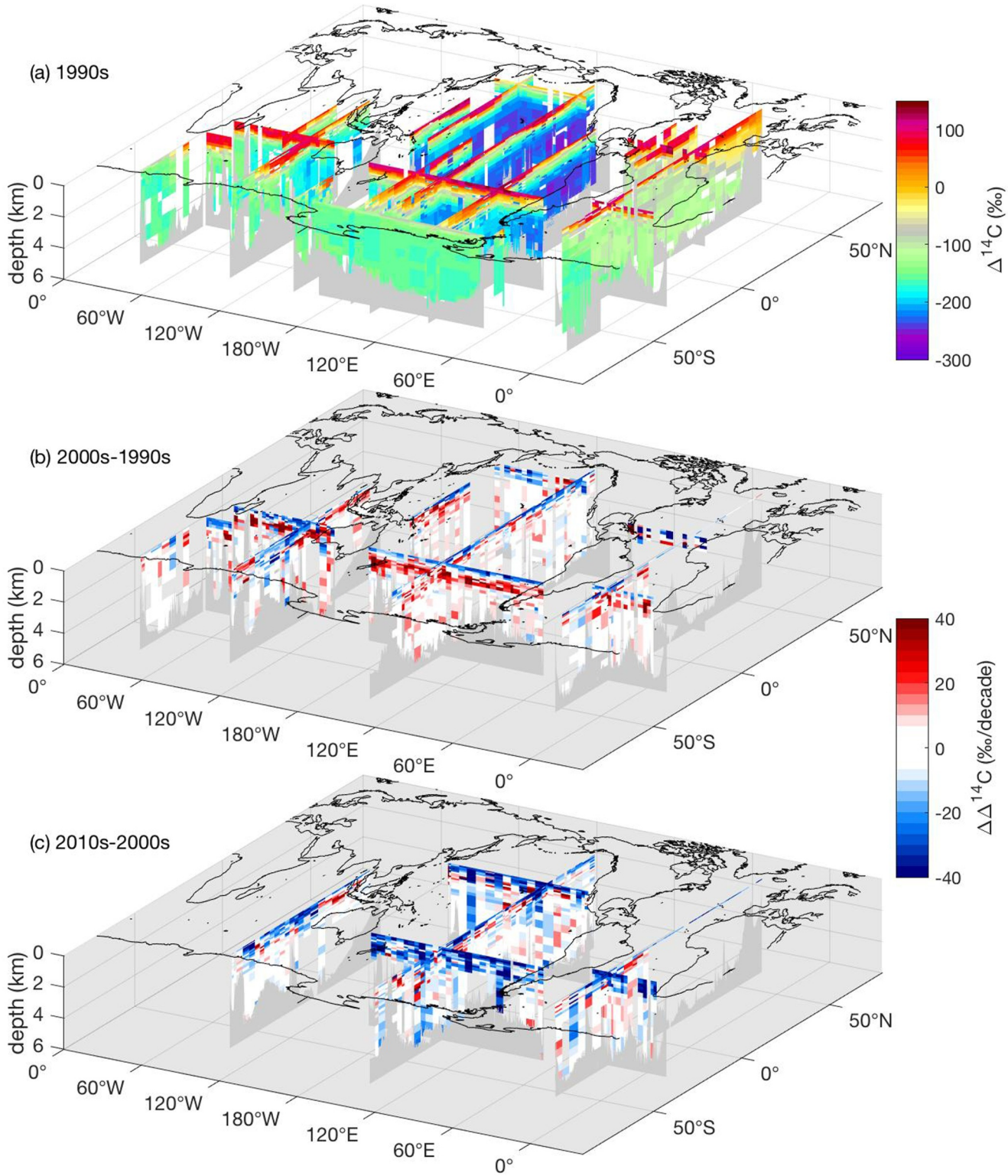

Figure 5. Observed ocean $\Delta^{14}C$ from the 1990 to the 2010s. (a) $\Delta^{14}C$ for the 1990s, (b) $\Delta\Delta^{14}C$ for the 1990–2000s, and (c) $\Delta\Delta^{14}C$ from the 2000 to 2010s.

Supporting Information S1) making reference to CFCs (Figure S8 in Supporting Information S1), then we compare subsurface biases for all tracers (Figure 9 and Figures S9–S19 in Supporting Information S1). The decreasing trend in surface $\Delta^{14}C$ between the 1970 and 2010s and the decrease in the spatial gradients in $\Delta^{14}C$

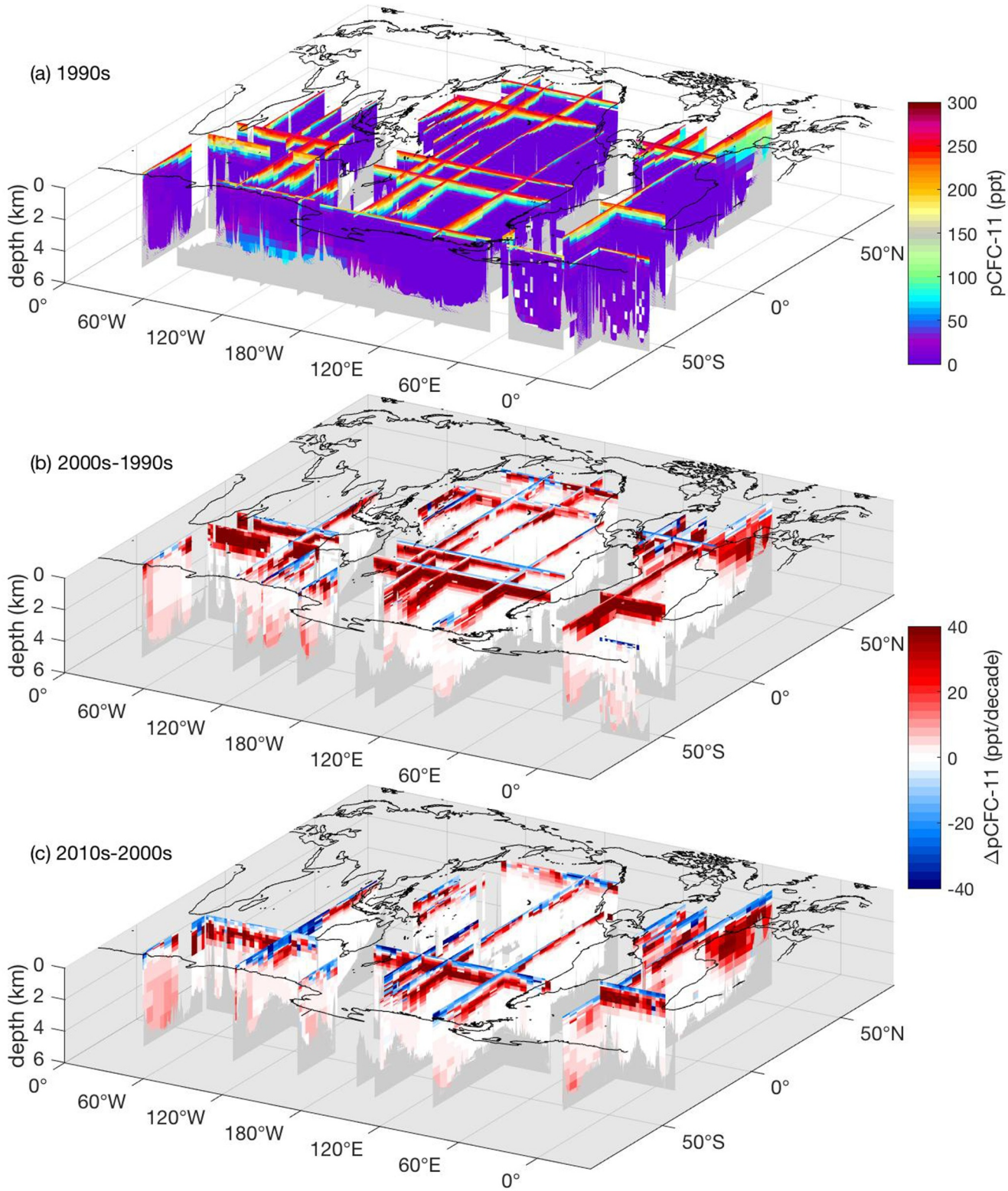

Figure 6. Observed ocean pCFC-11 from the 1990 to the 2010s. (a) pCFC-11 for the 1990s, (b) ΔpCFC-11 for 1990–2000s, and (c) ΔpCFC-11 for 2000–2010s.

seen in Figure 5 are again evident in Figures 8a–8d and Figure S6 in Supporting Information S1. The meridional surface $\Delta^{14}C$ bias trends for CESM2 tend to be flatter than the observations (Figure 4 and Figure S6 in Supporting Information S1). ECCOv4-TM is closer to the observations, with an RMS error of 25‰ in ECCOv4-TM and

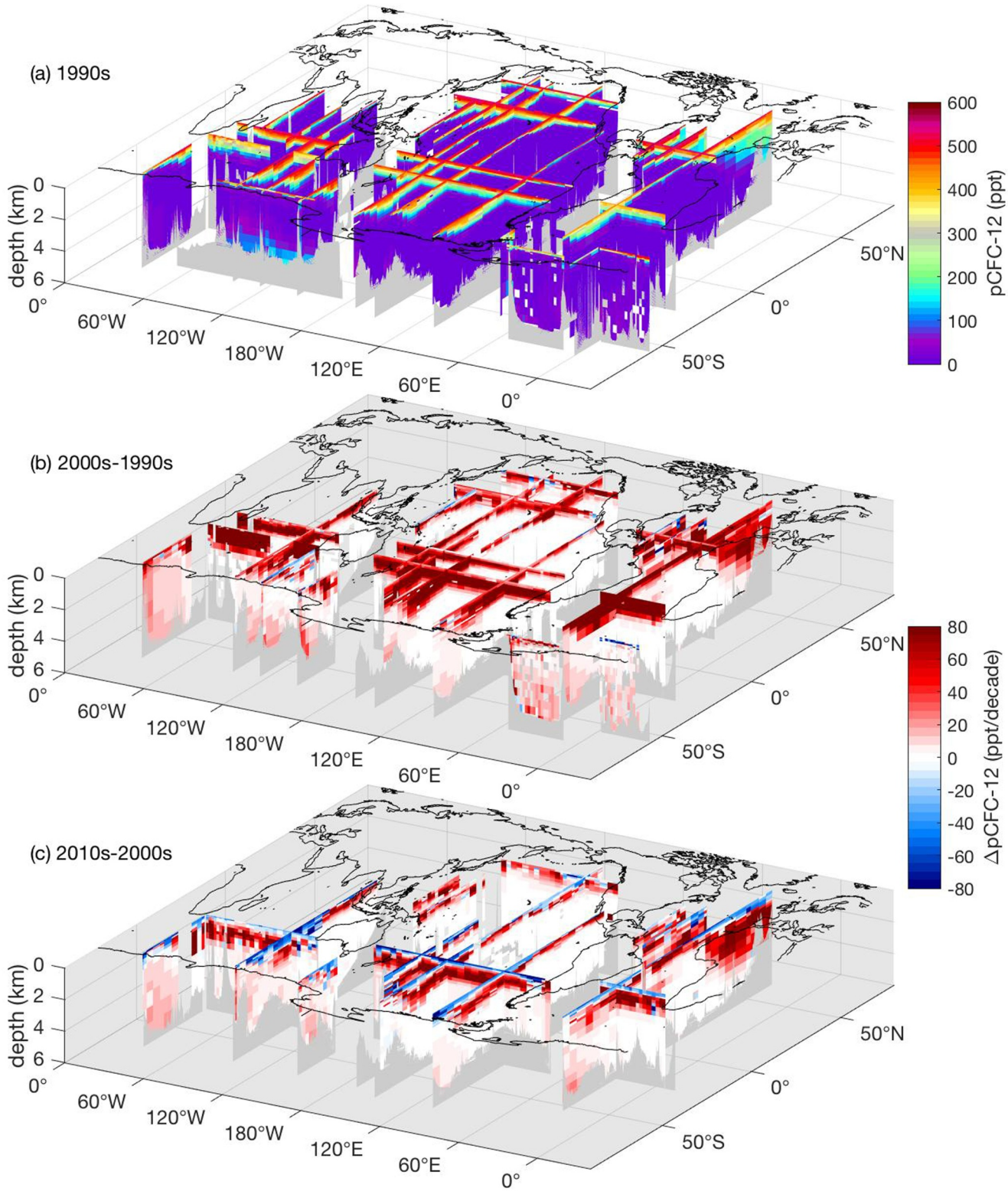

Figure 7. Observed ocean pCFC-12 from the 1990 to the 2010s. (a) pCFC-12 for the 1990s, (b) ΔpCFC-12 for 1990–2000s, and (c) ΔpCFC-12 for 2000–2010s.

33‰ in CESM2 for all surface $\Delta^{14}C$ observations (compared with RMS errors of 24‰ for ECCOv4-TM and 50‰ for CESM2 across all observations). Absolute biases in ECCOv4-TM are smaller than CESM2 in the Southern Ocean and North Atlantic Ocean, but larger in the Indian Ocean (Figure 8). Similar patterns can be seen

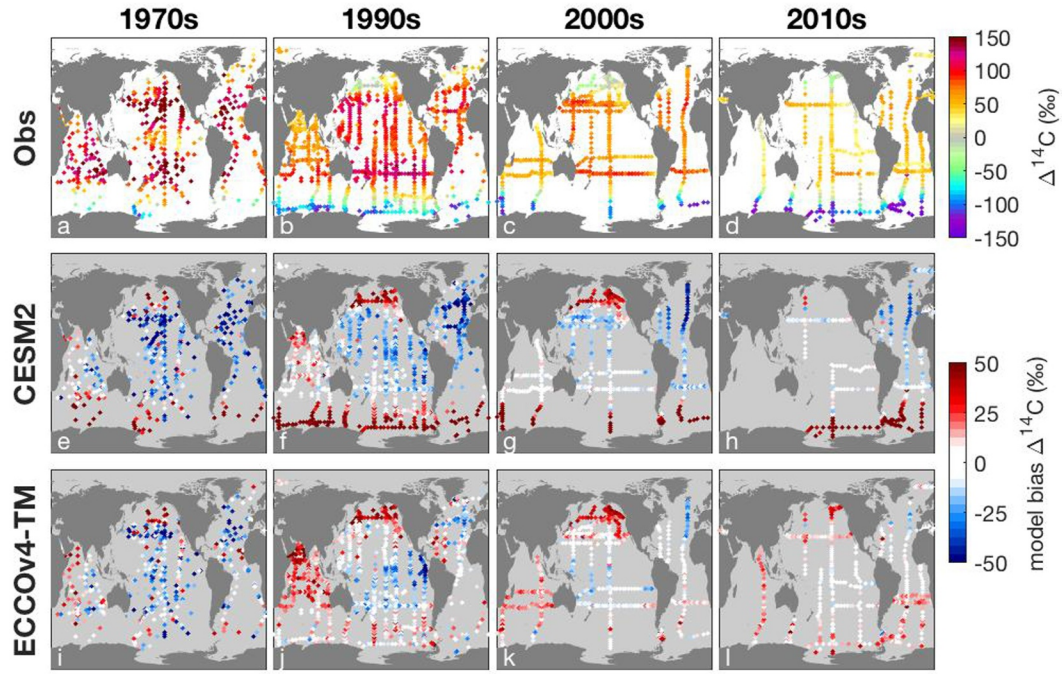

Figure 8. Surface ocean $\Delta^{14}C$ observations and model biases (model minus observations) from each ocean model. CESM2 outputs are only available until 2014, so cruises from 2014 onwards do not appear in panel (h).

in a comparison of clustered surface $\Delta^{14}C$ data from Toggweiler et al. (2019b) overlain on surface $\Delta^{14}C$ simulations from CESM2 and ECCOv4-TM (Figure S7 in Supporting Information S1).

The Indian Ocean being positively biased in ECCOv4-TM in the 1990–2010s could be caused by poor model representation of the upwelling which takes place in the Arabian Sea (Bhushan et al., 2008), also found by Toggweiler et al. (2019b) in a different selection of models. In CESM2 and ECCOv4-TM we see the same potential relocation of upwelling in the Indian Ocean from the Arabian Sea to the Bay of Bengal, as reported in Toggweiler et al. (2019b).

Both CESM2 and ECCOv4-TM are strongly positively biased in surface $\Delta^{14}C$ in the North Pacific. This finding echoes that of Toggweiler et al. (2019b), where they report large positive biases of surface $\Delta^{14}C$ in the North Pacific in their CM2Mc model, which they attribute to an erroneous poleward flow of high $\Delta^{14}C$ subtropical water along the California coast, opposite to the real-life southward flowing California Current.

North of 30°N in the Atlantic both CESM2 and ECCOv4-TM are too low in surface $\Delta^{14}C$ (Figure 8). The same deficit pattern is seen in the models from Toggweiler et al. (2019b), which they attribute to the fact that the return (northward) flow of NADW in their models is not brought to the surface in the tropical Atlantic, meaning not enough bomb ^{14}C is transported into the North Atlantic. However, we also see a strong positive bias in the subsurface North Atlantic in both CESM2 and ECCOv4-TM, which could perhaps also indicate too-vigorous mixing and NADW formation transported ^{14}C away from the surface (Figures S10 and S14 in Supporting Information S1).

Both CESM2 and ECCOv4-TM show negative biases in the tropical and subtropical upwelling regions of the Pacific Ocean in the 1970 and 1990s that dissipate through the 2010s (Figure 8). Unlike the Toggweiler et al. (2019b) models, CESM2 and ECCOv4-TM both capture the upwelling in South America in the pre-bomb era (Figure S7 in Supporting Information S1), although the model-data comparison in the 1990 and 2000s in these upwelling regions is poor, suggesting a similar source water problem as proposed in Toggweiler et al. (2019b). The upwelling regions in the eastern Atlantic have too high $\Delta^{14}C$ in both models in all time periods, suggesting either the upwelling is too weak or upwelled water is from the wrong source. CESM2 captures the $\Delta^{14}C$ observed gradient of around 10‰–15‰ between the east and western Pacific, but ECCOv4-TM has a higher gradient around 20‰, similar to Toggweiler et al. (2019b).

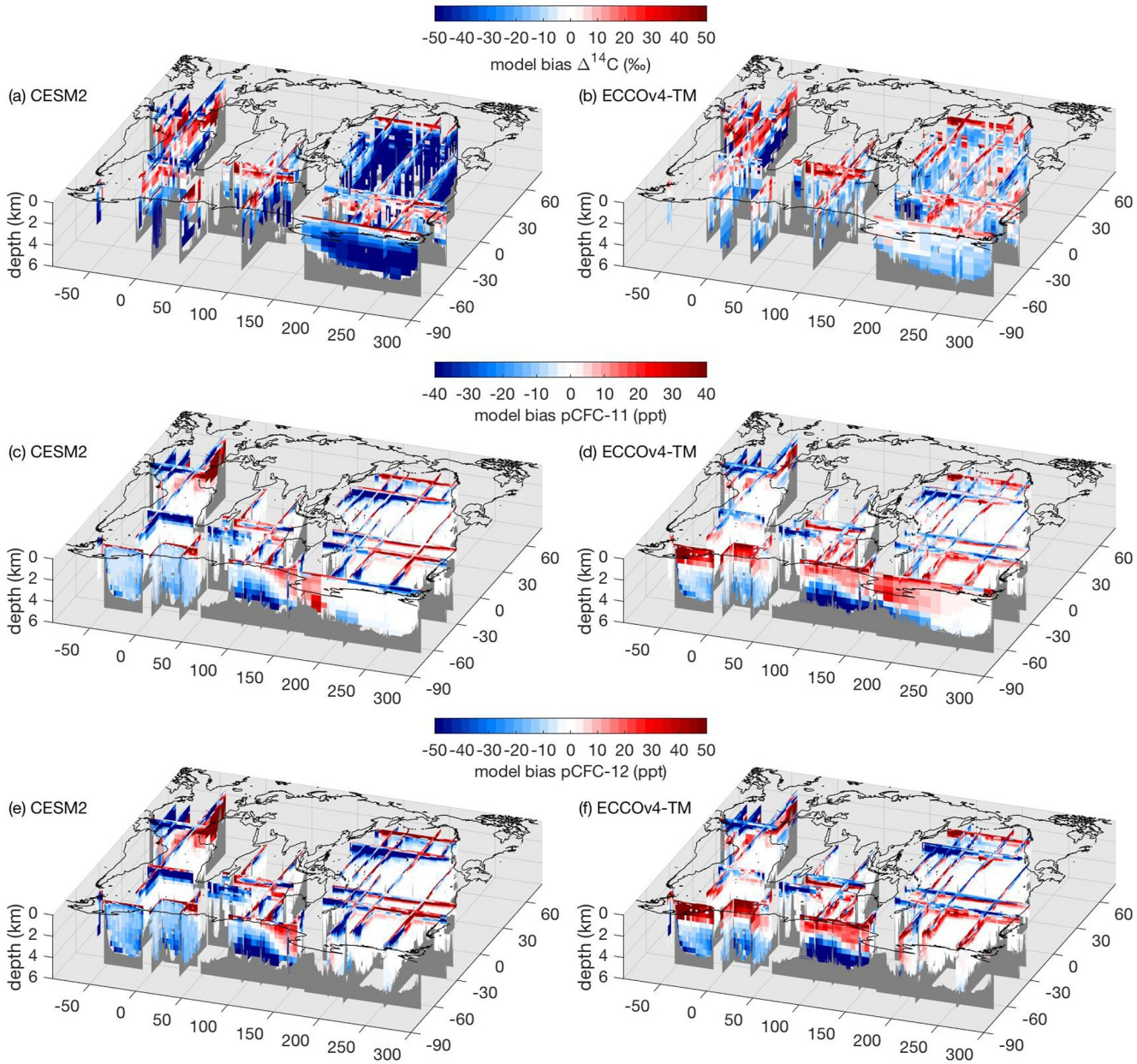

Figure 9. Model bias (model minus observations) for each tracer in the 1990s. Model bias for $\Delta^{14}C$ (top row), pCFC-11 (middle row), and pCFC-12 (bottom row), for CESM2 (left column) and ECCOv4-TM (right column).

Model biases in surface ocean pCFC are usually small since the fast equilibration time for CFCs in the ocean means that the surface ocean pCFC tracks the atmospheric values fairly closely. Using this fact, we examined apparent saturation in surface pCFC (Figure S8 in Supporting Information S1) to help identify anomalous values in the pCFC observations and select pCFC data to exclude (Table S3 in Supporting Information S1).

Vertical sections of ocean wide model biases help explain surface biases, and show that model biases for $\Delta^{14}C$ and CFCs are not always consistent (Figure 9). For instance, in the Indian subtropical gyre (I03), modeled surface radiocarbon is positively biased in both models, but pCFCs are negatively biased in both models (Figure S13 in Supporting Information S1). In the northwestern Pacific (P02), in CESM2 surface pCFC-11 is positively biased while pCFC-12 is negatively biased, and the biases are reversed in ECCOv4-TM (Figure S17 in Supporting Information S1). A prominent feature is the strong negative $\Delta^{14}C$ bias in CESM2 throughout the deep ocean but

most notably in the Pacific (Figures S10–S12 in Supporting Information S1), which stems from AABW formation in the CESM2 being too weak (Danabasoglu et al., 2020; Frischknecht et al., 2022). This also leads to potential densities in the deep Pacific that are too shallow in CESM2 (Figure S11 in Supporting Information S1). In contrast, the data-constrained ECCOv4-TM circulation generally keeps the potential density close to the observations and $\Delta^{14}C$ biases are much smaller. A prominent feature in the deeper waters of ECCOv4-TM is the strong negative $\Delta^{14}C$ bias along the western boundaries of the Indian (I05W) and Pacific (P06) basins (Figure 9b, Figures S13 and S18 in Supporting Information S1).

In the north Pacific, both models' pCFC tends to be positively biased in the sub-surface western subpolar gyre (P01, Figures 9c–9f and Figure S16 in Supporting Information S1), and negatively biased in the sub-surface western subtropical gyre (P02, Figures 9c–9f and Figure S17 in Supporting Information S1). The pairing may suggest a general tendency in our ocean models to ventilate the intermediate subpolar gyre with CFC-rich North Pacific Intermediate Water (Watanabe et al., 1994; Yamamoto-Kawai et al., 2004), which should instead be spreading beneath the subtropical gyre (Bostock et al., 2010; Talley, 1993). Alternatively, the subsurface dipole bias could due to the erroneous modeled poleward currents of equatorial water identified in Toggweiler et al. (2019b), transporting high $\Delta^{14}C$ and CFC water into the western subpolar gyre rather than the western subtropical gyre. A similar western intensified negative bias pattern is evident in all tracers in both zonal and meridional sections in all the subtropical gyres (Figures 9c–9f), which could indicate downwelling in the gyres is too weak in the models.

All modeled tracers in meridional sections of Antarctic Intermediate Water (AAIW) appear too high in ECCOv4-TM and too low in CESM2, indicating opposite biases in ventilation rates between models (Figure 9). All tracers are strongly positively biased in NADW in CESM2, and to a lesser extent in ECCOv4-TM, at 2000 m depth and north of 40°N (Figure 9, Figures S10 and S14 in Supporting Information S1).

The biases in $\Delta^{14}C$ in ECCOv4-TM and CESM2 are generally smaller than previous studies, except for the deep ocean globally and all depths of the Southern Ocean in CESM2. Matsumoto et al. (2004) found that fewer than a quarter of OCMIP-2 models fell within observational error bars for modeling $\Delta^{14}C$ in different regions in the ocean. Interestingly, deep ocean $\Delta^{14}C$ biases in Matsumoto et al. (2004) were mostly positive, as were the deep ocean biases in ECCO, an earlier version of ECCOv4-TM (Graven et al., 2012), opposite to the biases we find here in ECCOv4-TM and CESM2. CESM2 and ECCOv4-TM both appear to represent progress in model development, as their biases are generally smaller than their preceding versions CCSM, an earlier version of CESM, was found to have too high surface $\Delta^{14}C$ throughout the low and temperate latitudes (Graven et al., 2012). CCSM also had negative biases in $\Delta^{14}C$ in the Southern Ocean and deep ocean, but not as low as CESM2 (Graven et al., 2012). Previous studies have shown positive and negative biases in CFCs but detailed multi-model evaluations have not been reported since OCMIP-2 in the early 2000s (Dutay et al., 2002; Matsumoto et al., 2004), and only four models reported CFC output to CMIP6 (Fu et al., 2022).

3.3. Tracer Changes in Specific Regions

Here we describe in more detail the observed tracer changes and their comparison with models in specific regions: the Southern Ocean, the North Atlantic, the North Pacific, and the tropical oceans. We present additional figures for the Southern Ocean and North Atlantic, and refer to the summary figures (Figures 5–9) and supplemental figures for all regions. The figures detailing individual transects follow a consistent pattern. The tracers are shown in rows ordered in the sequence $\Delta^{14}C$, pCFC-11 then pCFC-12. The decadal tracer changes shown in the red-blue panels on the left, correspond with their zonally/meridionally averaged line profile partner on the right. Tracer changes are presented in decadal pairs (when there are three decades of available data), so the first row in each pair shows tracer changes from the 1990 to the 2000s, and the second row shows changes from the 2000 to the 2010s. The zonally/meridionally averaged observed line profiles then allow for comparison to the global average profiles presented in Figure 3.

3.3.1. Tracer Changes in the Southern Ocean

Decadal tracer changes in zonal sections circling the Southern Ocean near 30°S (A10/A9.5, I03, I05, and P06) are presented in Figure 10 (see also Kumamoto et al., 2011). Positive tracer changes are maximum around 500 m for pCFCs for the 1990–2000s, and the maximum changes are weaker and deeper for the 2000–2010s. For $\Delta^{14}C$, the maximum change is from 500 to 1,000 m for the 1990–2000s. For the 2000–2010s there is no coherent positive

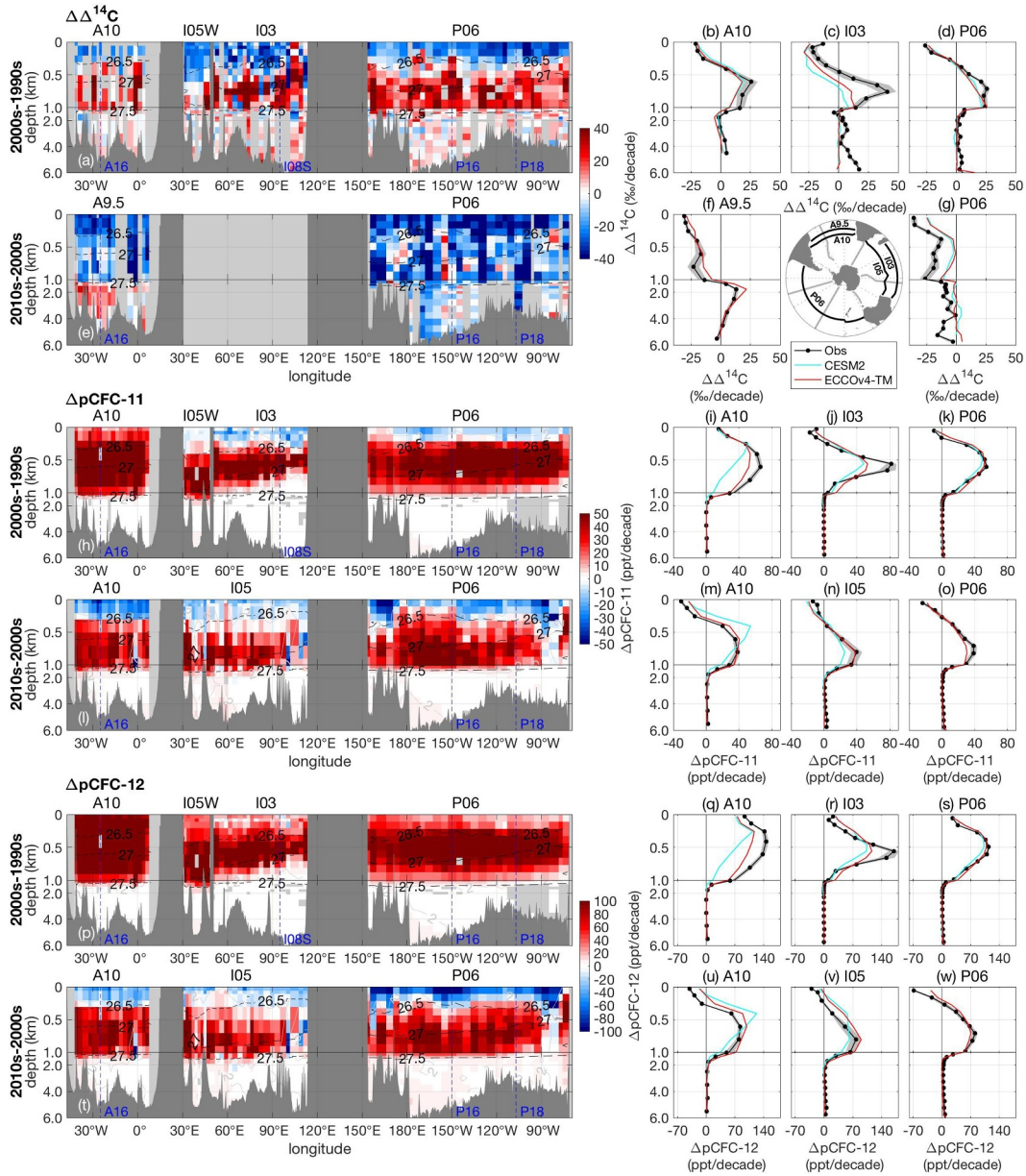

Figure 10. Changes in observed and modeled $\Delta^{14}C$ and pCFCs in the zonal Southern Ocean (A10, I05W, I03, and P06), over the last three decades. The first, third, and fifth rows show decadal tracer differences from 1990 to 2000s, the second, fourth and sixth rows show decadal tracer differences from 2000 to 2010s. The left column shows the observed zonal-depth sections, and the right three columns show the zonally averaged depth profiles for observations, and models CESM2 and ECCOv4-TM. Dashed black lines in the left column show potential density contours. Dashed blue lines and labels show where meridional sections intersect.

change in the south Pacific (P06) but there is a small area of $\Delta^{14}C$ increase observed for the South Atlantic (A9.5), where enhanced $\Delta^{14}C$ begins to appear in NADW in the western part of the section. Negative tracer changes in shallow waters get stronger for the 2000–2010s compared to the 1990–2000s for pCFC-11 and $\Delta^{14}C$. Positive $\Delta\Delta^{14}C$ observed in waters deeper than 3,000 m along I03 and negative $\Delta\Delta^{14}C$ observed in waters deeper than 3,000 m along P06 may result from the binning of sparse observations, or analytical offsets between different observations (Figures 10c and 10g).

The CESM2 and ECCOv4-TM models generally capture the patterns of section-average tracer change (right columns in Figure 10), however, they often underestimate the magnitude. In particular, positive $\Delta\Delta^{14}C$ and ΔpCFC in A10 and I03 from the 1990–2000s are stronger and have sharper maxima in the observations than in the

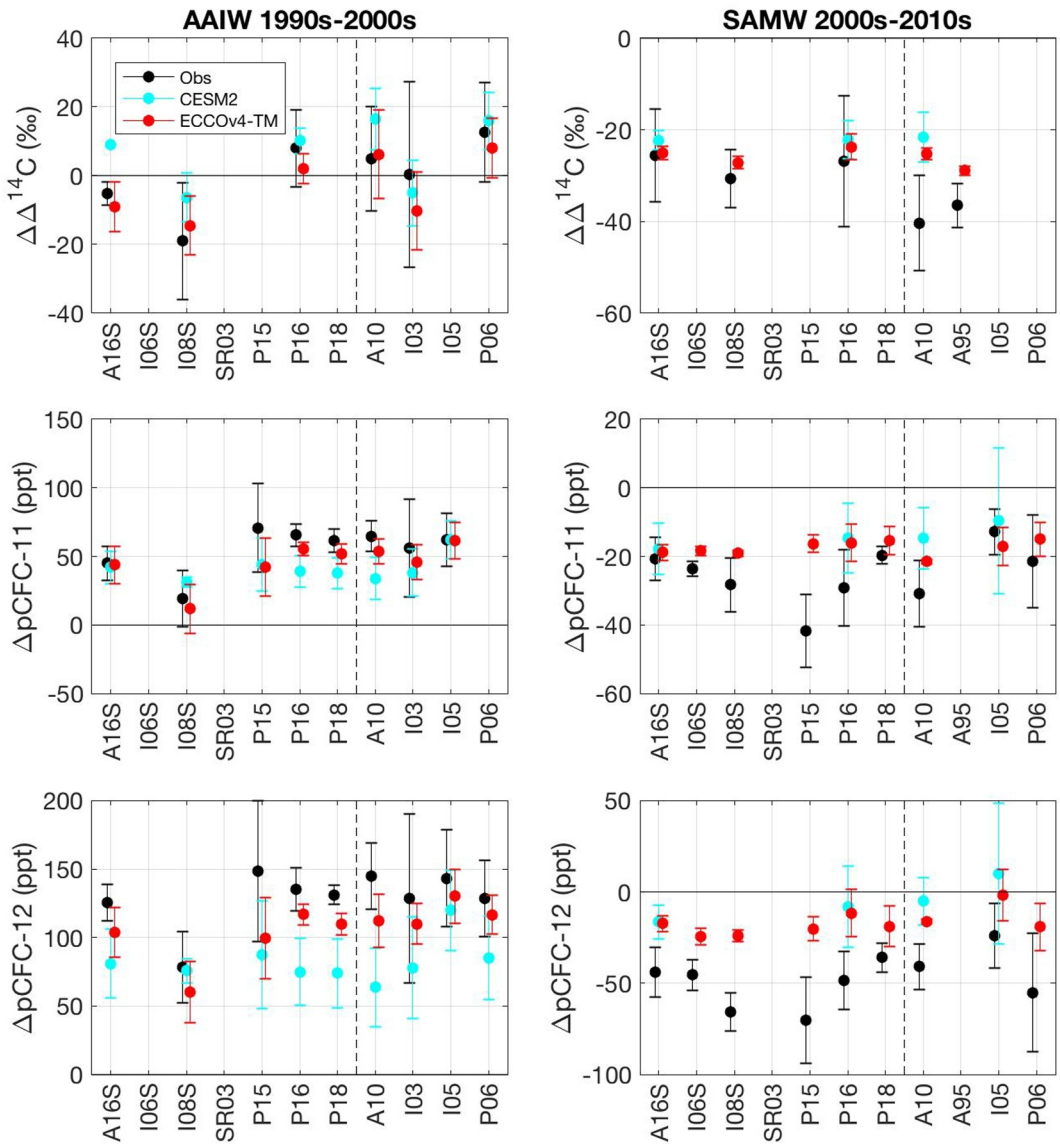

Figure 11. Southern Ocean $\Delta\Delta^{14}C$, ΔpCFC-11, and ΔpCFC-12 section averages for "AAIW" water for the 1990–2000s (left column, 26.5 to 27 σ_θ, 40°S to 30°S) and for "SAMW" water mass for the 2000–2010s (right column, 24 to 26 σ_θ, 50°S to 20°S). Zonal sections are shown on the right of the dashed line and meridional sections on the left. Error bars show the standard deviation across the water mass. For full zonal sections see Figure 10 and for full meridional sections see Figure S20–S22 in Supporting Information S1.

models (Figures 10i and 10j). The negative $\Delta\Delta^{14}C$ and ΔpCFC in shallower SAMW from the 2000–2010s are stronger in the observations than the models in all three basins. To draw out this feature, Figure 11 shows the average tracer changes in AAIW between the 1990–2000s and in SAMW for the 2000–2010s for all Southern Ocean sections. A tendency for underestimated magnitude in tracer changes in the models is coherent across multiple sections. The signal is less clear for $\Delta\Delta^{14}C$ in AAIW between the 1990–2000s, but those changes are near zero. Underestimated magnitude of tracer changes in SAMW and AAIW in these periods may indicate that the models are missing temporal variation in ventilation that may be driven by variation or trends in Southern Hemisphere winds (Swart & Fyfe, 2012; Waugh et al., 2013, 2019). The ECCOv4-TM simulation uses fixed circulation and while the CESM2 simulation does have varying circulation, it was run as a coupled model that may have a different realization of natural variability, which has been shown to be a primary factor for decadal tracer changes (Lester et al., 2020).

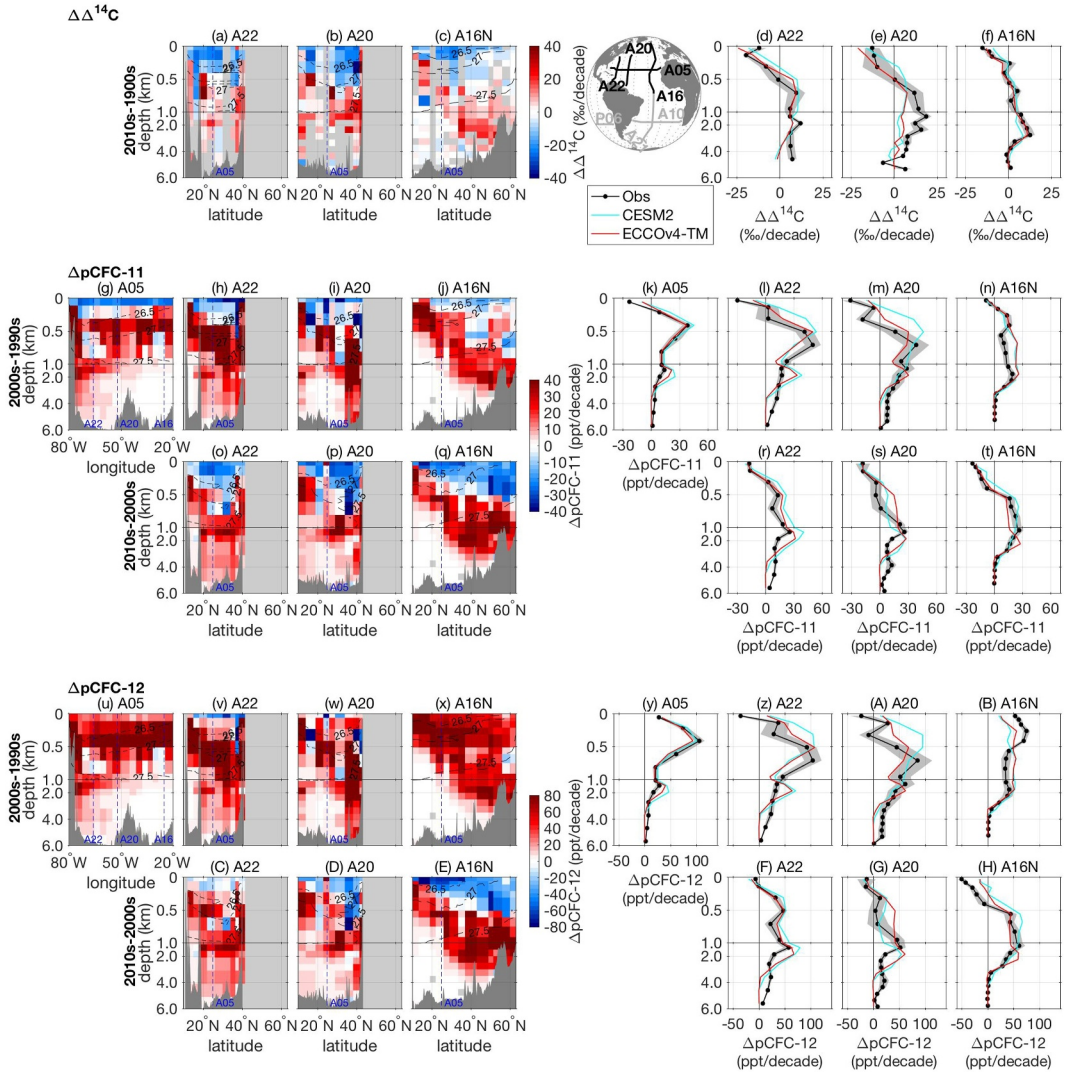

Figure 12. Changes in observed and modeled $\Delta^{14}C$ and chlorofluorocarbons in the North Atlantic (A05, A22, A20, and A16N) over the last three decades. $\Delta\Delta^{14}C$ from 1990 to 2010s, note only differences across two decades are shown due to limited data (first row), ΔpCFC-11 from 1990 to 2000s (second row), ΔpCFC-11 from 2000 to 2010s (third row), ΔpCFC-12 from 1990 to 2000s (fourth row), ΔpCFC-12 from 2000 to 2010s (fifth row). The left four columns show observed zonal- or meridional-depth sections, and the right four columns show the zonal- or meridionally averaged depth profiles for observations, and models CESM2 and ECCOv4-TM. Dashed black lines show potential density contours. Dashed blue lines and labels show where other sections intersect.

3.3.2. Tracer Changes in the North Atlantic Ocean

In the North Atlantic, very few $\Delta^{14}C$ observations were made in the 2000s, so we show differences between the 1990 and 2010s only (Figure 12). Differences in pCFCs are shown for each decade, as before, since there are sufficient pCFC data.

In shallow waters of the North Atlantic, $\Delta\Delta^{14}C$ and ΔpCFC-11 are both negative from the 1990–2000s, while ΔpCFC-12 is positive, as found elsewhere and in line with their atmospheric histories (Figure 12). In the 2000–2010s, negative shallow ΔpCFC-11 is stronger than the previous decade and extends deeper into the water column, while ΔpCFC-12 has changed sign from positive to negative due to the changing atmospheric history.

At depth, all three tracers illustrate the southward passage of tracer ventilated NADW in the western Atlantic (e.g., Smethie et al., 2000). This is evidenced by the strong ΔpCFC from the 1990–2000s in the west of A05 down to 4,000 m (Figures 12g and 12u) and in the westernmost meridional section A22. In sections A20 and A16 further to the east, strong ΔpCFC at depth is only present in the northernmost parts. Some $\Delta^{14}C$ measurements were taken

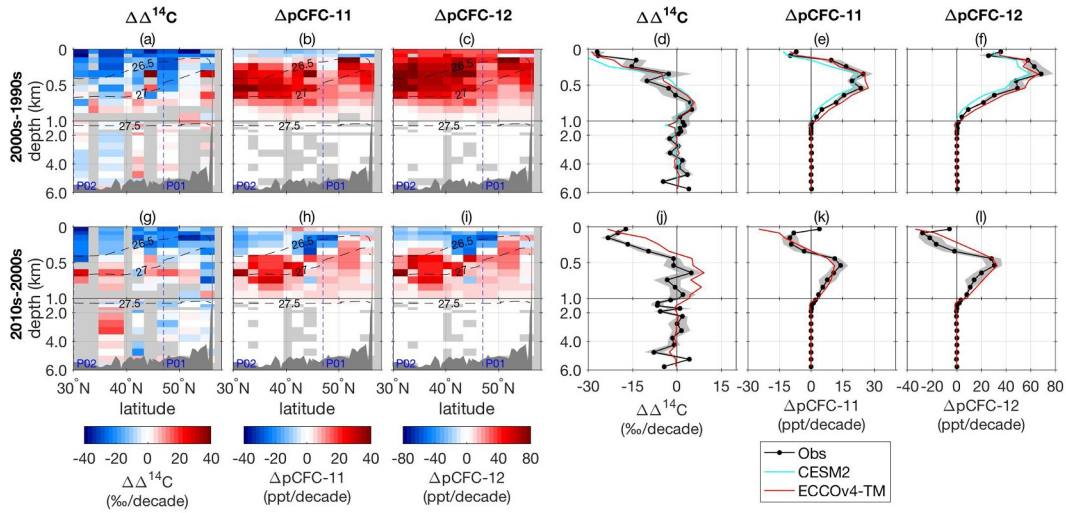

Figure 13. Changes in observed and modeled $\Delta^{14}C$ and chlorofluorocarbons along P16 in the North Pacific over the last three decades. Top row shows decadal differences from 1990 to 2000s, bottom row shows decadal differences from 2000 to 2010s. The left three columns show observed meridional-depth sections, and the right three columns show the meridionally averaged depth profiles for observations, and models CESM2 and ECCOv4-TM. Dashed black lines show potential density contours. Dashed blue lines and labels show where zonal sections intersect.

along A05 in 1992 but they are too sparse to represent large-scale changes so only A22, A20, and A16 are shown for $\Delta^{14}C$ in Figure 12.

The sections A22, A20, and A05 emphasize that bomb-$\Delta^{14}C$ and CFCs in NADW are being carried below 3,500 m in the western Atlantic, in contrast to the shallower, more concentrated core centered at ~2,000 m in the models (Figures 12l, 12m, 12r, 12s, 12z, 12A, 12F, and 12G). This shallow bias may have consequences for other ocean basins, as demonstrated by the ocean-wide negative bias in $\Delta^{14}C$ in both models deeper than 3,000 m (Figures 9a and 9b). In contrast, the depth that tracer changes go to zero in the eastern Atlantic (A16, ~3,000 m) is well-captured by the models.

In shallower waters above 2,000 m, the models most often simulate ΔpCFC that is too positive, including shallow waters down to 500 m in the western Atlantic from the 1990–2000s (A20 and A22, Figures 12l, 12m, 12z, and 12A). This model bias is also hinted at in the western Atlantic $\Delta\Delta^{14}C$ change between the 1990 and 2010s (Figures 12d and 12e), but it disappears for ΔpCFCs from the 2000 to the 2010s. ΔpCFC between 500 and 3,000 m at A20 from the 2000–2010s and A16 from the 1990–2000s appears much more constant with depth in the models than in the observations. Interestingly, at A16N, ΔpCFC-11 above 500 m is well-captured by the models in both time periods while ΔpCFC-12 above 500 m is too low for 1990–2000s and too high for 2000–2010s. One source of variability in ΔpCFC here that may not be captured by the models is the North Atlantic Oscillation, which has been found to affect the uptake of anthropogenic carbon along A05 (Brown et al., 2010).

3.3.3. Tracer Changes in the North Pacific Ocean

Shallow ocean $\Delta\Delta^{14}C$ observations in the North Pacific are consistent with other regions in both time periods, with negative $\Delta\Delta^{14}C$ between −20‰ and −30‰ per decade observed in shallow waters (Figures 13a and 13g). Coherent $\Delta^{14}C$ increases are found in deeper layers (600–1,000 m) for the 1990–2000s, but not for the 2000–2010s. Despite the strong positive model bias of $\Delta^{14}C$ in the shallow North Pacific (Figure 8), the models largely capture the decadal decrease in $\Delta^{14}C$ in the upper 500 m, although the models are slightly weaker than the observations in the 2000–2010s (Figures 13d and 13j). However, only a few sections have repeat $\Delta^{14}C$ measurements in the North Pacific and only the meridional P16 section has measurements in all three decades, which restricts the analysis of decadal changes (Figure 5).

The ΔpCFC observations at P16 are generally consistent with other regions in both time periods (Figure 13), except for the abrupt positive ΔpCFC-11 and zero ΔpCFC-12 observed in the upper 100 m from the 2000–2010s, which could be a seasonal feature (also observed at P10 and P09, Figure S23 in Supporting Information S1). In the

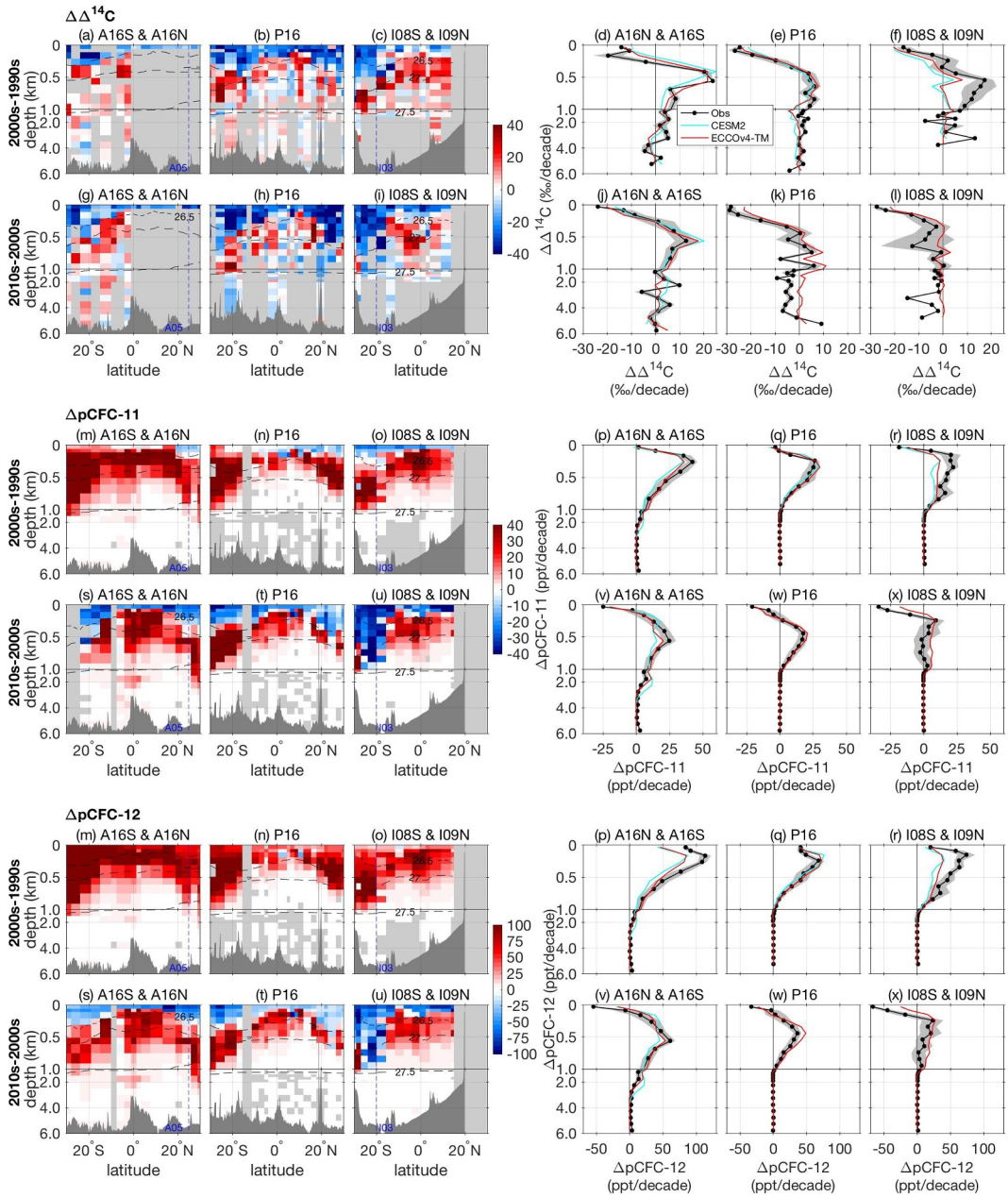

Figure 14. Changes in observed and modeled $\Delta^{14}C$ and chlorofluorocarbons in the meridional tropical Atlantic (A16), Pacific (P16), and Indian (I08S and I09N) oceans, over the last three decades. The first, third, and fifth rows shows decadal tracer differences from 1990 to 2000s, the second, fourth, and sixth rows shows decadal tracer differences from 2000 to 2010s. The left three columns show observed meridional-depth sections, and the right three columns show the meridionally averaged depth profiles for observations, and models CESM2 and ECCOv4-TM. Dashed black lines show potential density contours. Dashed blue lines and labels show where meridional sections intersect.

North Pacific the simulated pCFCs tend to be positively biased in the subpolar gyre, and negatively biased in subtropical gyre (Figure 8), but the models capture the ΔpCFC well at P16 (Figure 13). As previously mentioned in Section 2.1, CFCs were measured at numerous other transects in the North Pacific (e.g., P01, P02, P09, P10, P13, and P15), but those sections were excluded because they appear to show inconsistencies in at least one time period (Figures S4 and S5 and Table S3 in Supporting Information S1).

3.3.4. Tracer Changes in the Tropical Oceans

As expected by the strong thermocline in the tropics, the tracer changes are restricted to the top 1,500 m (Figure 14). Increases in $\Delta^{14}C$ between the 1990 and 2000s and the 2000 and 2010s are apparent in all three basins in the tropical lower thermocline, in contrast to higher latitudes where such increases were not observed between the 2000 and 2010s. Profiles in the Indian Ocean from the 2000–2010s differ to the other two basins as there is a region centered around 20°S where all three tracers decrease between the surface and 1,000 m (Figures 14i, 14u, and 14G). The latitude of this feature corresponds approximately to the Indonesian throughflow and South Equatorial Current, suggesting it may result from the transport of Pacific waters. Simulated average changes in the tracers with depth are generally consistent with the models in the Atlantic and Pacific, but not in the Indian Ocean where the changes between are too weak in the models, throughout the water column for CFCs, but only between 400 and 1,000 m for $\Delta^{14}C$. The feature observed in the Indian Ocean could potentially relate to variability from the Indian Ocean Dipole that is not captured in the models.

4. Discussion

Measurements of the major ocean tracers $\Delta^{14}C$, CFC-11, and CFC-12 over the past three decades show that we have entered an era of large-scale decreases of all tracers over time in the ocean, consistent with their decline in the atmosphere. There are now few regions in the ocean where $\Delta^{14}C$ is increasing, and the regions with increasing CFC-11 and CFC-12 are similarly becoming restricted to smaller and deeper areas as their atmospheric declines continue. These declines are motivating an increase in the measurement of SF_6 in the ocean, which continues to grow in the atmosphere and therefore can largely replace CFCs in some applications (e.g., Tanhua et al., 2013). However, $\Delta^{14}C$, CFC-11, and CFC-12 measurements, used alone or in concert with other tracers, can continue to be of great utility for model evaluation, study of ocean circulation (Toggweiler et al., 2019b) and detection of ocean circulation variability (Pookkandy et al., 2023), as well as in applications estimating anthropogenic CO_2 uptake (Graven et al., 2012).

Critical to the continued utility of these tracers, particularly as ocean tracer changes weaken in magnitude, is the precision and comparability of measurements made at different points in time and by different laboratories. There were numerous sections (summarized in Table S3 in Supporting Information S1) that we chose not to present detailed analysis for CFCs due to questions about the data. Notably, along P02 and P01 there appears to be offsets in pCFC between different cruise legs in some cases. P13 showed unexpected patterns in decadal pCFC change with depth that could possibly indicate evidence of CFC contamination during the 2001 cruise (Figure S5 in Supporting Information S1). Similar extremes are not seen in $\Delta^{14}C$, but in a few cases (P6, P10) there are some unexpectedly large differences between decades in the deep ocean that point to potential measurement offsets, and there are far fewer sections available for comparison. This indicates that data products such as GLODAP may need more careful evaluation and/or adjustment before they are utilized in inversions or other data analysis.

The two state-of-the-art models we use here reveal a general pattern that negative tracer changes in the upper ocean are often weaker in the models than the observations since the 1990s (Figures 10 and 12). This is true for $\Delta^{14}C$ and both pCFCs. This may relate to biases in model mean transport, but it could also be consistent with a reduction in vertical transport and mixing due to ocean warming-induced stratification in the observations. Model experiments varying the strength of upper ocean warming and stratification would be useful to test this hypothesis. Other areas where model biases appear to be linked with ocean circulation changes are in the Southern Ocean, consistent with other studies (Waugh et al., 2013). In the deep sea, model biases appear to relate to errors in the mean circulation, such as the underestimate of deep ocean ventilation and $\Delta^{14}C$ (Figures 8 and 9), the depth that NADW extends to (Figures 9 and 12), and the upwelling in the Indian Ocean and North Pacific Ocean (Figures 8 and 9).

Comparing our model-data evaluation to that from Toggweiler et al. (2019b), we find a broad agreement in most of the surface $\Delta^{14}C$ bias patterns they identify. CESM2 and ECCOv4-TM seem to better capture the pre-bomb upwelling $\Delta^{14}C$ patterns on the west coast of the Americas and Africa then the models in Toggweiler et al. (2019b), but show similar depleted surface $\Delta^{14}C$ in subsequent decades, which would be consistent with the upwelled water not having been ventilated with enough $\Delta^{14}C$ as suggested by Toggweiler et al. (2019b). We also see a negative bias in $\Delta^{14}C$ increasing to the west of the Pacific, which could be consistent with the too-weak spreading of upwelled SAMW/AAIW origin waters proposed in Toggweiler et al. (2019b).

The importance of continuing to measure these tracers in the ocean is demonstrated by many other studies. Khatiwala et al. (2018) showed how the oceanic radiocarbon distribution is projected to completely reverse over this century. However, simulated future $\Delta^{14}C$ changes are moderated by simulated future changes in the Atlantic Meridional Overturning Circulation (Khatiwala et al., 2018), which $\Delta^{14}C$ and CFC data may help to detect. Since air-sea ^{14}C fluxes are a strong influence on $\Delta^{14}C$ gradients in atmospheric CO_2, oceanic data are needed for studies of atmospheric $\Delta^{14}C$ that, for example, aim to quantify fossil fuel emissions (Basu et al., 2020). As noted by Eglinton et al. (2023), there is a need for sustaining and building up observation networks for $\Delta^{14}C$ measurement across carbon reservoirs to understand the global carbon cycle. In addition, predicted future outgassing of CFCs will influence CFC lifetimes and stratospheric ozone, as well as detection of illegal CFC emissions (Wang et al., 2021).

There is an acute absence of tracer data in certain locations. Data are not available to monitor the re-emergence of SAMW in the upwelling regions in North and South America proposed in Toggweiler et al. (2019a, 2019b), which may reframe the oceanic outflows between basins. Fine upwelling structures revealed by the dense surface data during the WOCE era remain obscure voids in the more recent decades. While the dense sampling undertaken during the 1990s continue to stand as a benchmark against which models need to perform, continued measurements are needed to investigate the complex puzzle of natural and anthropogenic ocean circulation changes.

The two models we present in this study do not allow for the study of circulation change responses in CFCs and $\Delta^{14}C$. However, recent work by Pookkandy et al. (2023) using the NEMO ocean model in $\Delta^{14}C$ simulations with fixed or variable climate forcing found that circulation changes resulted in $\Delta^{14}C$ signals that were larger than the typical $\Delta^{14}C$ measurement uncertainty, indicating that $\Delta^{14}C$ data should be applied in studies of circulation changes. So far, tracer data-driven studies of circulation change have focused on CFCs and SF_6 (e.g., Cimoli et al., 2023; Fine et al., 2017; Mecking et al., 2006; Tanhua et al., 2013; Waugh et al., 2013), where CFCs will continue to be useful in coming decades.

The overview of three decades of tracer data we show here represents a vast collaborative effort by seagoing and laboratory scientists, supported by many countries and programs. We hope that by presenting the data together here we help to inspire more studies on these existing data, as well as continued investment in future measurements that will tell the continuing story of these tracers in the sea, as they make their way into the ocean interior and respond to changes in ocean circulation.

5. Conclusions

We present a global overview of ocean radiocarbon and CFC measurements conducted over the last three decades, and compare these observations to two ocean circulation models. The observations show that average surface ocean $\Delta^{14}C$ continues to decrease from the 2000–2010s at an average of 20‰ per decade in response to decreasing atmospheric $\Delta^{14}C$, shallow-to-deep mixing, and the efflux of ^{14}C. Bomb ^{14}C that initially accumulated in the shallow ocean continues to disperse, with a corresponding reduction in extent and magnitude of $\Delta^{14}C$ increase at depth. Recent trends in upper ocean $\Delta^{14}C$, pCFC-11, and pCFC-12 are negative, reflecting their decreasing atmospheric trends, with the onset of the negative trend beginning later for pCFC-12.

Ocean models largely capture the observed patterns in tracer distribution and tracer changes but show biases in some areas, and the tracer changes observed hint at significant decadal variations in some areas that are not captured by either the fixed circulation (ECCOv4-TM) or coupled (CESM2) models. In addition, the model-data comparisons indicate a too-shallow depth of the NADW in the western North Atlantic in both models and underestimates of the magnitude of tracer changes in Antarctic Intermediate Water from the 1990 to the 2000s and in Subantarctic Mode Water from the 2000 to the 2010s. In general, the models underestimate the decreasing trends in all the tracers in the shallow ocean, while simulating increases in $\Delta^{14}C$ at depth that are only detected in the observations in a few places. These biases may indicate signals of stratification in the tracer observations, or biases in the model transport.

Detection of tracer changes, particularly for $\Delta^{14}C$, are limited by data availability and measurement precision and comparability. For example, sub-surface decadal changes in $\Delta^{14}C$ in the North Atlantic cannot be characterized because no measurements were conducted there in the 2000s. For some sections, implied tracer changes indicate issues with measurement comparability. As the radiocarbon and CFC tracers will continue to evolve in the ocean

as the atmospheric composition changes, our study highlights the need for sustained investment in and careful curation of $\Delta^{14}C$ and CFC measurements to ensure the continued utility of these tracers to ocean science. Our results also reiterate the importance of simulating radiocarbon in ocean and climate models. While radiocarbon has long been recognized as a powerful constraint on large scale ocean circulation (e.g., Matsumoto et al., 2004), natural ^{14}C is computationally expensive to simulate. Thus, only a very small handful of CMIP6 models included it in their runs. Recently developed approaches to accelerate such simulations (Khatiwala, 2023) may encourage more modeling groups to simulate radiocarbon in future CMIP exercises.

Data Availability Statement

Ocean tracer data are available from GLODAP (https://www.glodap.info/) (Key et al., 2015; Olsen et al., 2016, 2019), with additional data available from the CCHDO (https://cchdo.ucsd.edu/) (Curry, 2012; Druffel, 2016; King, 2018; Macdonald, 2016; Macdonald & Briggs, 2018; McCartney, 2012; Mecking & Rosso, 2018; Orsi & Rosso, 2020; Perkin, 1999; Rintoul, 2018; Speer & Schulze, 2018; Volkov & Menezes, 2018), NCEI (https://www.ncei.noaa.gov) (Barbero et al., 2018; Baringer et al., 2016) and JAMSTEC (https://doi.org/10.17596/0000032) (Uchida et al., 2011). The TMM code, ECCOv4-TM transport matrices and related forcing data are available from Khatiwala (2018) (https://zenodo.org/record/1246300). ECCOv4-TM modeled tracer simulations are available from Lester (2023) (https://zenodo.org/record/8242144). CESM2 modeled tracer simulations are available from NCAR's Earth System Grid (https://www.earthsystemgrid.org/dataset/ucar.cgd.cesm2.output.html) (Danabasoglu et al., 2020).

Acknowledgments

We are indebted to the hundreds of sea-going and laboratory scientists and crew who conducted the tracer measurements, and made their data available. Likewise the many scientists who contributed to the development and simulations of the earth system models used here. We acknowledge funding from the Leverhulme Trust and from the Natural Environment Research Council under Grants NE/P019242/1 to H.G. and NE/P019218/1 to S.K. for the Transient tracer-based Investigation of Circulation and Thermal Ocean Change (TICTOC) project. SK was also supported by NERC Grant NE/W007258/1. J.L. was supported by the Grantham Institute SSCP DTP, Grant NE/L002515/1. We would like to thank Robert (Bob) Key for his invaluable contribution to the collection and compilation of oceanic radiocarbon data over the last few decades, and for his advice regarding some of the radiocarbon data used in this study. Reviews by R. E. Sonnerup, K. Matsumoto, and J. R. Toggweiler greatly improved the paper.

References

Barbero, L., Wanninkhof, R., Dickson, A. G., Carlson, C. A., Key, R. M., Becker, S., et al. (2018). Discrete profile measurements of dissolved inorganic carbon, total alkalinity, pH on total scale and other hydrographic and chemical data obtained during R/V Roger Revelle repeat hydrography cruise in the Indian ocean: GO-SHIP section I09N (EXPOCODE 33RR20160321), from 2016-03-21 to 2016-04-28 (NCEI accession 0178637) [Dataset]. *NOAA National Centers for Environmental Information*. https://doi.org/10.25921/f59c-dy18

Baringer, M. O., Bullister, J. L., Feely, R. A., Wanninkhof, R., Millero, F. J., Hansell, D. A., et al. (2016). Dissolved inorganic carbon (DIC), total alkalinity, pH on seawater scale, partial pressure of carbon dioxide (pCO2), dissolved organic carbon (DOC), chlorofluorocarbons (CFC-11, CFC-12), temperature, salinity and other hydrographic and chemical variables collected from discrete samples and profile observations during NOAA Ship Ronald H. Brown cruise CLIVAR_A16N_2013 (EXPOCODE 33RO20130803) in the Atlantic Ocean from 2013-08-03 to 2013-10-01 (NCEI Accession 0157363) [Dataset]. *NOAA National Centers for Environmental Information*. https://doi.org/10.3334/cdiac/otg.goship_a16n_2013

Basu, S., Lehman, S. J., Miller, J. B., Andrews, A. E., Sweeney, C., Gurney, K. R., et al. (2020). Estimating US fossil fuel CO_2 emissions from measurements of ^{14}C in atmospheric CO_2. *Proceedings of the National Academy of Sciences of the United States of America*, *117*(24), 13300–13307. https://doi.org/10.1073/pnas.1919032117

Bhushan, R., Dutta, K., & Somayajulu, B. (2008). Estimates of upwelling rates in the Arabian Sea and the equatorial Indian Ocean based on bomb radiocarbon. *Journal of Environmental Radioactivity*, *99*(10), 1566–1571. https://doi.org/10.1016/j.jenvrad.2007.12.006

Bostock, H. C., Opdyke, B. N., & Williams, M. J. M. (2010). Characterising the intermediate depth waters of the Pacific Ocean using $\delta^{13}C$ and other geochemical tracers. *Deep Sea Research Part I*, *57*(7), 847–859. https://doi.org/10.1016/j.dsr.2010.04.005

Broecker, W., & Peng, T. H. (1974). Gas exchange rates between air and sea. *Tellus*, *26*(1–2), 21–35. https://doi.org/10.3402/tellusa.v26i1-2.9733

Brown, P. J., Bakker, D. C., Schuster, U., & Watson, A. J. (2010). Anthropogenic carbon accumulation in the subtropical North Atlantic. *Journal of Geophysical Research*, *115*(C4). https://doi.org/10.1029/2008jc005043

Bullister, J. L. (2015). Atmospheric histories (1765–2015) for CFC-11, CFC-12, CFC-113, CCl4, SF6 and N2O, carbon dioxide information analysis center [Dataset]. *Oak Ridge National Laboratory, US Department of Energy*. https://doi.org/10.3334/cdiac/otg.cfc_atm_hist_2015

Chapman, P. (1998). The world ocean circulation experiment (WOCE). *Marine Technology Society Journal*, *32*(3), 23–36.

Cimoli, L., Gebbie, G., Purkey, S. G., & Smethie, W. M. (2023). Annually resolved propagation of CFCs and SF_6 in the global ocean over eight decades. *Journal of Geophysical Research: Oceans*, *128*(3), e2022JC019337. https://doi.org/10.1029/2022jc019337

Craig, H. (1972). The GEOSECS program: 1970–1971. *Earth and Planetary Science Letters*, *16*(1), 47–49. https://doi.org/10.1016/0012-821x(72)90235-x

Craig, H. (1974). The geosecs program: 1972–1973. *Earth and Planetary Science Letters*, *23*(1), 63–64. https://doi.org/10.1016/0012-821X(74)90031-4

Craig, H., & Turekian, K. (1976). The GEOSECS program: 1973–1976. *Earth and Planetary Science Letters*, *32*(2), 217–219. https://doi.org/10.1016/0012-821x(76)90062-5

Craig, H., & Turekian, K. (1980). The GEOSECS program: 1976–1979. *Earth and Planetary Science Letters*, *49*(2), 263–265. https://doi.org/10.1016/0012-821x(80)90071-0

Curry, R. (2012). Bottle data from Cruise 33AT20120324, exchange version [Dataset]. *CCHDO*. https://cchdo.ucsd.edu/cruise/33AT20120324

Danabasoglu, G., Lamarque, J., Bacmeister, J., Bailey, D. A., DuVivier, A. K., Edwards, J., et al. (2020). The community earth system model version 2 (CESM2). *Journal of Advances in Modeling Earth Systems*, *12*(2), e2019MS001916. https://doi.org/10.1029/2019ms001916

DeVries, T., & Primeau, F. (2011). Dynamically and observationally constrained estimates of water-mass distributions and ages in the global ocean. *Journal of Physical Oceanography*, *41*(12), 2381–2401. https://doi.org/10.1175/JPO-D-10-05011.1

Doney, S. C., & Bullister, J. L. (1992). A chlorofluorocarbon section in the eastern North Atlantic. *Deep-Sea Research, Part A: Oceanographic Research Papers*, *39*(11–12), 1857–1883. https://doi.org/10.1016/0198-0149(92)90003-c

Druffel, E. (2016). Bottle data from Cruise 33RO20110926, exchange version [Dataset]. *CCHDO*. https://cchdo.ucsd.edu/cruise/33RO20110926

Dutay, J.-C., Bullister, J. L., Doney, S. C., Orr, J. C., Najjar, R., Caldeira, K., et al. (2002). Evaluation of ocean model ventilation with CFC-11: Comparison of 13 global ocean models. *Ocean Modelling*, *4*(2), 89–120. https://doi.org/10.1016/s1463-5003(01)00013-0

Eglinton, T. I., Graven, H. D., Raymond, P. A., Trumbore, S. E., Aluwihare, L., Bard, E., et al. (2023). Making the case for an international decade of radiocarbon. *Philosophical Transactions of the Royal Society A*, *381*(2261), 20230081. https://doi.org/10.1098/rsta.2023.0081

Eyring, V., Bony, S., Meehl, G. A., Senior, C. A., Stevens, B., Stouffer, R. J., & Taylor, K. E. (2016). Overview of the coupled model Intercomparison project phase 6 (CMIP6) experimental design and organization. *Geoscientific Model Development*, *9*(5), 1937–1958. https://doi.org/10.5194/gmd-9-1937-2016

Fine, R. A. (2011). Observations of CFCs and SF_6 as ocean tracers. *Annual Review of Marine Science*, *3*(1), 173–195. https://doi.org/10.1146/annurev.marine.010908.163933

Fine, R. A., Peacock, S., Maltrud, M. E., & Bryan, F. O. (2017). A new look at ocean ventilation time scales and their uncertainties. *Journal of Geophysical Research: Oceans*, *122*(5), 3771–3798. https://doi.org/10.1002/2016JC012529

Forget, G., Campin, J. M., Heimbach, P., Hill, C. N., Ponte, R. M., & Wunsch, C. (2015). ECCO version 4: An integrated framework for non-linear inverse modeling and global ocean state estimation. *Geoscientific Model Development*, *8*(10), 3071–3104. https://doi.org/10.5194/gmd-8-3071-2015

Frischknecht, T., Ekici, A., & Joos, J. (2022). Radiocarbon in the land and ocean components of the community earth system model. *Global Biogeochemical Cycles*, *36*(1), e2021GB007042. https://doi.org/10.1029/2021GB007042

Fu, W., Moore, J. K., Primeau, F., Collier, N., Ogunro, O. O., Hoffman, F. M., & Randerson, J. T. (2022). Evaluation of ocean biogeochemistry and carbon cycling in CMIP earth system models with the International Ocean Model Benchmarking (IOMB) software system. *Journal of Geophysical Research: Oceans*, *127*(10), e2022JC018965. https://doi.org/10.1029/2022jc018965

Graven, H., Allison, C. E., Etheridge, D. M., Hammer, S., Keeling, R. F., Levin, I., et al. (2017). Compiled records of carbon isotopes in atmospheric CO_2 for historical simulations in CMIP6. *Geoscientific Model Development*, *10*(12), 4405–4417. https://doi.org/10.5194/gmd-10-4405-2017

Graven, H. D. (2015). Impact of fossil fuel emissions on atmospheric radiocarbon and various applications of radiocarbon over this century. *Proceedings of the National Academy of Sciences*, *112*(31), 9542–9545. https://doi.org/10.1073/pnas.1504467112

Graven, H. D., Gruber, N., Key, R., Khatiwala, S., & Giraud, X. (2012). Changing controls on oceanic radiocarbon: New insights on shallow-to-deep ocean exchange and anthropogenic CO_2 uptake. *Journal of Geophysical Research*, *117*(C10), C10005. https://doi.org/10.1029/2012JC008074

Graven, H. D., Keeling, R., & Xu, X. (2022). Radiocarbon dating: Going back in time. *Nature*, *607*(7919), 449. https://doi.org/10.1038/d41586-022-01954-y

Holzer, M., Primeau, F. W., Smethie, W. M., Jr., & Khatiwala, S. (2010). Where and how long ago was water in the western North Atlantic ventilated? Maximum entropy inversions of bottle data from WOCE line A20. *Journal of Geophysical Research*, *115*(C7), C07005. https://doi.org/10.1029/2009JC005750

Key, R. M. (2001). Radiocarbon. In *Encyclopedia of ocean sciences* (pp. 2338–2353).

Key, R. M., Kozyr, A., Sabine, C. L., Lee, K., Wanninkhof, R., Bullister, J. L., et al. (2004). A global ocean carbon climatology: Results from global data analysis project (GLODAP). *Global Biogeochemical Cycles*, *18*(4), GB4031. https://doi.org/10.1029/2004gb002247

Key, R. M., Olsen, A., van Heuven, S., Lauvset, S., Velo, A., Lin, X., et al. (2015). Global Data Analysis Project, Version 2 (GLODAPv2). ORNL/CDIAC-162, NDP-093, Carbon Dioxide Information Analysis Center, Oak Ridge National Laboratory, US Department of Energy, Oak Ridge, Tennessee.

Khatiwala, S. (2007). A computational framework for simulation of biogeochemical tracers in the ocean. *Global Biogeochemical Cycles*, *21*(3), GB3001. https://doi.org/10.1029/2007gb002923

Khatiwala, S. (2008). Fast spin up of ocean biogeochemical models using matrix-free Newton-Krylov. *Ocean Modelling*, *23*(3–4), 121–129. https://doi.org/10.1016/j.ocemod.2008.05.002

Khatiwala, S. (2018). Transport Matrix Method software for ocean biogeochemical simulations [Software]. *Zenodo*. https://doi.org/10.5281/zenodo.1246300

Khatiwala, S. (2023). Fast spin-up of geochemical tracers in ocean circulation and climate models. *Journal of Advances in Modeling Earth Systems*, *15*(2), e2022MS003447. https://doi.org/10.1029/2022MS003447

Khatiwala, S., Graven, H., Payne, S., & Heimbach, P. (2018). Changes to the air-sea flux and distribution of radiocarbon in the Ocean over the 21st century. *Geophysical Research Letters*, *45*(11), 5617–5626. https://doi.org/10.1029/2018GL078172

Khatiwala, S., Primeau, F., & Hall, T. (2009). Reconstruction of the history of anthropogenic CO_2 concentrations in the ocean. *Nature*, *462*(7271), 346–349. https://doi.org/10.1038/nature08526

Khatiwala, S., Primeau, F., & Holzer, M. (2012). Ventilation of the deep ocean constrained with tracer observations and implications for radiocarbon estimates of ideal mean age. *Earth and Planetary Science Letters*, *325*(326), 116–125. https://doi.org/10.1016/j.epsl.2012.01.038

Khatiwala, S., Visbeck, M., & Cane, M. (2005). Accelerated simulation of passive tracers in ocean circulation models. *Ocean Modelling*, *9*(1), 51–69. https://doi.org/10.1016/j.ocemod.2004.04.002

King, B. (2018). Bottle data from Cruise 740H20180228, exchange version [Dataset]. *CCHDO*. https://cchdo.ucsd.edu/cruise/740H20180228

Kumamoto, Y., Murata, A., Watanabe, S., & Fukasawa, M. (2011). Temporal and spatial variations in bomb-produced radiocarbon along BEAGLE2003 lines—Revisits of WHP P06, A10, and I03/I04 in the Southern Hemisphere Oceans. *Progress in Oceanography*, *89*(1–4), 49–60. https://doi.org/10.1016/j.pocean.2010.12.007

Large, W. G., & Yeager, S. G. (2009). The global climatology of an interannually varying air–sea flux data set. *Climate Dynamics*, *33*(2–3), 341–364. https://doi.org/10.1007/s00382-008-0441-3

Lester, J. G. (2023). Changes in oceanic radiocarbon and CFCs since the 1990s [Dataset]. *Zenodo*. https://doi.org/10.5281/zenodo.8242144

Lester, J. G., Lovenduski, N. S., Graven, H. D., Long, M. C., & Lindsay, K. (2020). Internal variability dominates over externally forced ocean circulation changes seen through CFCs. *Geophysical Research Letters*, *47*(9), e2020GL087585. https://doi.org/10.1029/2020gl087585

Li, X., & Primeau, F. (2008). A fast Newton-Krylov solver for seasonally varying global ocean biogeochemistry models. *Ocean Modelling*, *23*(1–2), 13–20. https://doi.org/10.1016/j.ocemod.2008.03.001

Lindsay, K. (2017). A Newton–Krylov solver for fast spin-up of online ocean tracers. *Ocean Modelling*, *109*, 33–43. https://doi.org/10.1016/j.ocemod.2016.12.001

Macdonald, A. (2016). Bottle data from Cruise 33RR20160208, exchange version. [Dataset]. *CCHDO*. https://cchdo.ucsd.edu/cruise/33RR20160208

Macdonald, A., & Briggs, E. (2018). Bottle data from Cruise 320620180309, exchange version [Dataset]. *CCHDO*. https://doi.org/10.7942/C2F08X

Manning, M. R., Lowe, D. C., Melhuish, W. H., Sparks, R. J., Wallace, G., Brenninkmeijer, C. A. M., & McGill, R. C. (1990). The use of radiocarbon measurements in atmospheric studies. *Radiocarbon*, *32*(1), 37–58. https://doi.org/10.1017/s0033822200039941

Marshall, J., Adcroft, A., Hill, C., Perelman, L., & Heisey, C. (1997). A finite-volume, incompressible Navier Stokes model for studies of the ocean on parallel computers. *Journal of Geophysical Research*, *102*(C3), 5753–5766. https://doi.org/10.1029/96JC02775

Matsumoto, K., Sarmiento, J. L., Key, R. M., Aumont, O., Bullister, J. L., Caldeira, K., et al. (2004). Evaluation of ocean carbon cycle models with data-based metrics. *Geophysical Research Letters*, *31*(7), L07303. https://doi.org/10.1029/2003gl018970

McCartney, M. (2012). Bottle data from Cruise 33AT20120419, exchange version [Dataset]. *CCHDO*. https://cchdo.ucsd.edu/cruise/33AT20120419

Mecking, S., & Rosso, I. (2018). Bottle data from Cruise 320620170703, exchange version [Dataset]. *CCHDO*. https://doi.org/10.7942/C2PH20

Mecking, S., Warner, M. J., & Bullister, J. L. (2006). Temporal changes in pCFC-12 ages and AOU along two hydrographic sections in the eastern subtropical North Pacific. *Deep Sea Research Part I: Oceanographic Research Papers*, *53*(1), 169–187. https://doi.org/10.1016/j.dsr.2005.06.018

Meinshausen, M., Nicholls, Z. R. J., Lewis, J., Gidden, M. J., Vogel, E., Freund, M., et al. (2020). The shared socio-economic pathway (SSP) greenhouse gas concentrations and their extensions to 2500. *Geoscientific Model Development*, *13*(8), 3571–3605. https://doi.org/10.5194/gmd-13-3571-2020

Meinshausen, M., Vogel, E., Nauels, A., Lorbacher, K., Meinshausen, N., Etheridge, D. M., et al. (2017). Historical greenhouse gas concentrations for climate modelling (CMIP6). *Geoscientific Model Development*, *10*(5), 2057–2116. https://doi.org/10.5194/gmd-10-2057-2017

Molina, M. J., & Rowland, F. S. (1974). Stratospheric sink for chlorofluoromethanes: Chlorine atom-catalysed destruction of ozone. *Nature*, *249*(5460), 810–812. https://doi.org/10.1038/249810a0

Müller, S., Joos, F., Edwards, N., & Stocker, T. (2006). Water mass distribution and ventilation time scales in a cost-efficient, three-dimensional ocean model. *Journal of Climate*, *19*(21), 5479–5499. https://doi.org/10.1175/jcli3911.1

Naegler, T. (2009). Reconciliation of excess ^{14}C-constrained global CO_2 piston velocity estimates. *Tellus B: Chemical and Physical Meteorology*, *61*(2), 372–384. https://doi.org/10.1111/j.1600-0889.2008.00408.x

Olsen, A., Key, R. M., van Heuven, S., Lauvset, S. K., Velo, A., Lin, X., et al. (2016). The Global Ocean Data Analysis Project version 2 (GLODAPv2)—An internally consistent data product for the world ocean [Dataset]. *Earth System Science Data*, *8*(2), 297–323. https://doi.org/10.5194/essd-8-297-2016

Olsen, A., Lange, N., Key, R. M., Tanhua, T., Álvarez, M., Becker, S., et al. (2019). GLODAPv2. 2019—An update of GLODAPv2. *Earth System Science Data*, *11*(3), 1437–1461. https://doi.org/10.5194/essd-11-1437-2019

Orr, J. C., Dutay, J., Najjar, R., Bullister, J., & Brockmann, P. (1999). CFC-HOWTO. Internal OCMIP Report (12 pp.). LSCE/CEA Saclay, Gif-sur-Yvette, France.

Orr, J. C., Najjar, R., Sabine, C. L., & Joos, F. (1999). Abiotic-HOWTO. Internal OCMIP Report (25 pp.). Lab. des Sci. du Clim. et l'Environ., Gif-sur-Yvette, France.

Orr, J. C., Najjar, R. G., Aumont, O., Bopp, L., Bullister, J. L., Danabasoglu, G., et al. (2017). Biogeochemical protocols and diagnostics for the CMIP6 Ocean Model Intercomparison project (OMIP). *Geoscientific Model Development*, *10*(6), 2169–2199. https://doi.org/10.5194/gmd-10-2169-2017

Orsi, A., & Rosso, I. (2020). Bottle data from Cruise 325020190403, exchange version [Dataset]. *CCHDO*. https://doi.org/10.7942/C29660

Perkin, R. (1999). Bottle data from Cruise 18DD199905_1, exchange version [Dataset]. CCHDO. Retrieved from https://cchdo.ucsd.edu/cruise/18DD199905_1

Pookkandy, B., Graven, H., & Martin, A. (2023). Contemporary oceanic radiocarbon response to ocean circulation changes. *Climate Dynamics*, *61*(7–8), 3223–3235. https://doi.org/10.1007/s00382-023-06737-3

Purkey, S. G., Smethie, W. M., Jr., Gebbie, G., Gordon, A. L., Sonnerup, R. E., Warner, M. J., & Bullister, J. L. (2018). A synoptic view of the ventilation and circulation of Antarctic Bottom Water from chlorofluorocarbons and natural tracers. *Annual Review of Marine Science*, *10*(1), 503–527. https://doi.org/10.1146/annurev-marine-121916-063414

Rintoul, S. (2018). Bottle data from Cruise 096U20180111, exchange version [Dataset]. *CCHDO*. https://cchdo.ucsd.edu/cruise/096U20180111

Rubin, S. I., & Key, R. M. (2002). Separating natural and bomb-produced radiocarbon in the ocean: The potential alkalinity method. *Global Biogeochemical Cycles*, *16*(4), 52-1–52-9. https://doi.org/10.1029/2001gb001432

Sabine, C. L., Feely, R. A., Gruber, N., Key, R. M., Lee, K., Bullister, J. L., et al. (2004). The oceanic sink for anthropogenic CO_2. *Science*, *305*(5682), 367–371. https://doi.org/10.1126/science.1097403

Smethie, W. M., Jr., Fine, R. A., Putzka, A., & Jones, E. P. (2000). Tracing the flow of North Atlantic Deep Water using chlorofluorocarbons. *Journal of Geophysical Research*, *105*(C6), 14297–14323. https://doi.org/10.1029/1999jc900274

Smith, R., Jones, P., Briegleb, B., Bryan, F., Danabasoglu, G., Dennis, J., et al. (2010). The parallel ocean program (POP) reference manual ocean component of the community climate system model (CCSM) and community earth system model (CESM), LAUR-10-01853, Los Alamos National Laboratory (141 pp.).

Speer, K., & Schulze, L. (2018). Bottle data from Cruise 320620170820, exchange version [Dataset]. *CCHDO*. https://doi.org/10.7942/C2JQ02

Stuiver, M., & Polach, H. A. (1977). Discussion: Reporting of ^{14}C data. *Radiocarbon*, *19*(3), 355–363. https://doi.org/10.1017/s0033822200003672

Swart, N. C., & Fyfe, J. C. (2012). Observed and simulated changes in the Southern Hemisphere surface westerly wind-stress. *Geophysical Research Letters*, *39*(16), D18101. https://doi.org/10.1029/2012gl052810

Sweeney, C., Gloor, E., Jacobson, A. R., Key, R. M., McKinley, G., Sarmiento, J. L., & Wanninkhof, R. (2007). Constraining global air-sea gas exchange for CO_2 with recent bomb ^{14}C measurements. *Global Biogeochemical Cycles*, *21*(2), GB2015. https://doi.org/10.1029/2006gb002784

Talley, L. D. (1993). Distribution and formation of North Pacific Intermediate Water. *Journal of Physical Oceanography*, *23*(3), 517–537. https://doi.org/10.1175/1520-0485(1993)023<0517:DAFONP>2.0.CO;2

Talley, L. D., Feely, R., Sloyan, B., Wanninkhof, R., Baringer, M., Bullister, J., et al. (2016). Changes in ocean heat, carbon content, and ventilation: A review of the first decade of GO-SHIP global repeat hydrography. *Annual Review of Marine Science*, *8*(1), 185–215. https://doi.org/10.1146/annurev-marine-052915-100829

Tanhua, T., Jones, E. P., Jeansson, E., Jutterström, S., Smethie, W. M., Jr., Wallace, D. W., & Anderson, L. G. (2009). Ventilation of the Arctic Ocean: Mean ages and inventories of anthropogenic CO_2 and CFC-11. *Journal of Geophysical Research*, *114*(C1), C01002. https://doi.org/10.1029/2008jc004868

Tanhua, T., Waugh, D. W., & Bullister, J. L. (2013). Estimating changes in ocean ventilation from early 1990s CFC-12 and late 2000s SF_6 measurements. *Geophysical Research Letters*, *40*(5), 927–932. https://doi.org/10.1002/grl.50251

Ting, Y.-H., & Holzer, M. (2017). Decadal changes in Southern Ocean ventilation inferred from deconvolutions of repeat hydrographies. *Geophysical Research Letters*, *44*(11), 5655–5664. https://doi.org/10.1002/2017GL073788

Toggweiler, J. R., Dixon, K., & Bryan, K. (1989). Simulations of radiocarbon in a coarse-resolution world ocean model. 1. Steady state prebomb distributions. *Journal of Geophysical Research*, *94*(C6), 8217–8242. https://doi.org/10.1029/jc094ic06p08217

Toggweiler, J. R., Druffel, E. R. M., Key, R. M., & Galbraith, E. D. (2019a). Upwelling in the ocean basins north of the ACC: 1. On the upwelling exposed by the surface distribution of $\Delta^{14}C$. *Journal of Geophysical Research: Oceans*, *124*(4), 2591–2608. https://doi.org/10.1029/2018jc014794

Toggweiler, J. R., Druffel, E. R. M., Key, R. M., & Galbraith, E. D. (2019b). Upwelling in the ocean basins north of the ACC: 2. How cool subantarctic water reaches the surface in the tropics. *Journal of Geophysical Research: Oceans*, *124*(4), 2609–2625. https://doi.org/10.1029/2018jc014795

Trenberth, K. (1999). The evolution of the CLIVAR Science. In *Proceedings of the international CLIVAR conference, WMO/TD-No. 954* (pp. 17–19). World Meteorological Organization-Publications.

Uchida, H., Murata, A., & Doi, T. (2011). WHP P21 revisit data book [Dataset]. *JAMSTEC*. https://doi.org/10.17596/0000032

van Vuuren, D. P., Edmonds, J., Kainuma, M., Riahi, K., Thomson, A., Hibbard, K., et al. (2011). The representative concentration pathways: An overview. *Climatic Change*, *109*(1–2), 5–31. https://doi.org/10.1007/s10584-011-0148-z

Volkov, D., & Menezes, V. (2018). Bottle data from Cruise 33RO20180423, exchange version [Dataset]. *CCHDO*. https://doi.org/10.7942/C25H2B

Wallace, D. W., & Lazier, J. R. (1988). Anthropogenic chlorofluoromethanes in newly formed Labrador Sea Water. *Nature*, *332*(6159), 61–63. https://doi.org/10.1038/332061a0

Wang, P., Scott, J. R., Solomon, S., Marshall, J., Babbin, A. R., Lickley, M., et al. (2021). On the effects of the ocean on atmospheric CFC-11 lifetimes and emissions. *Proceedings of the National Academy of Sciences USA*, *118*(12), e2021528118. https://doi.org/10.1073/pnas.2021528118

Wanninkhof, R. (1992). Relationship between wind speed and gas exchange over the ocean. *Journal of Geophysical Research*, *97*(C5), 7373–7382. https://doi.org/10.1029/92JC00188

Wanninkhof, R. (2014). Relationship between wind speed and gas exchange over the ocean revisited. *Limnology and Oceanography: Methods*, *12*(6), 351–362. https://doi.org/10.4319/lom.2014.12.351

Warner, M. J., & Weiss, R. F. (1985). Solubilities of chlorofluorocarbons 11 and 12 in water and seawater. *Deep-Sea Research, Part A: Oceanographic Research Papers*, *32*(12), 1485–1497. https://doi.org/10.1016/0198-0149(85)90099-8

Watanabe, Y. W., Harada, K., & Ishikawa, K. (1994). Chlorofluorocarbons in the central North Pacific and southward spreading time of North Pacific intermediate water. *Journal of Geophysical Research*, *99*(C12), 25195–25213. https://doi.org/10.1029/94JC01884

Waugh, D. W., Hogg, A. M. C., Spence, P., England, M. H., & Haine, T. W. N. (2019). Response of Southern Ocean ventilation to changes in midlatitude westerly winds. *Journal of Climate*, *32*(17), 5345–5361. https://doi.org/10.1175/JCLI-D-19-0039.1

Waugh, D. W., Primeau, F., DeVries, T., & Holzer, M. (2013). Recent changes in the ventilation of the southern oceans. *Science*, *339*(6119), 568–570. https://doi.org/10.1126/science.1225411

Weiss, R. F., Bullister, J. L., Gammon, R. H., & Warner, M. J. (1985). Atmospheric chlorofluoromethanes in the deep equatorial Atlantic. *Nature*, *314*(6012), 608–610. https://doi.org/10.1038/314608a0

Wunsch, C., & Heimbach, P. (2007). Practical global oceanic state estimation. *Physica D: Nonlinear Phenomena*, *230*(1–2), 197–208. https://doi.org/10.1016/j.physd.2006.09.040

Yamamoto-Kawai, M., Watanabe, S., Tsunogai, S., & Wakatsuchi, M. (2004). Chlorofluorocarbons in the Sea of Okhotsk: Ventilation of the intermediate water. *Journal of Geophysical Research*, *109*(C9), C09S11. https://doi.org/10.1029/2003JC001919

References From the Supporting Information

Adcroft, A., & Campin, J.-M. (2004). Rescaled height coordinates for accurate representation of free-surface flows in ocean circulation models. *Ocean Modelling*, *7*(3–4), 269–284. https://doi.org/10.1016/j.ocemod.2003.09.003

Danabasoglu, G., Bates, S. C., Briegleb, B. P., Jayne, S. R., Jochum, M., Large, W. G., et al. (2012). The CCSM4 ocean component. *Journal of Climate*, *25*(5), 1361–1389. https://doi.org/10.1175/JCLI-D-11-00091.1

Dee, D. P., Uppala, S. M., Simmons, A. J., Berrisford, P., Poli, P., Kobayashi, S., et al. (2011). The ERA-Interim reanalysis: Configuration and performance of the data assimilation system. *Quarterly Journal of the Royal Meteorological Society*, *137*(656), 553–597. https://doi.org/10.1002/qj.828

Gaspar, P., Grégoris, Y., & Lefevre, J.-M. (1990). A simple eddy kinetic energy model for simulations of the oceanic vertical mixing: Tests at station Papa and long-term upper ocean study site. *Journal of Geophysical Research*, *95*(C9), 16179–16193. https://doi.org/10.1029/JC095iC09p16179

Gent, P. R., & Mcwilliams, J. C. (1990). Isopycnal mixing in ocean circulation models. *Journal of Physical Oceanography*, *20*(1), 150–155. https://doi.org/10.1175/1520-0485(1990)020<0150:IMIOCM>2.0.CO;2

Hunke, E. C., Lipscomb, W. H., Turner, A. K., Jeffery, N., & Elliott, S. (2015). CICE: The Los Alamos sea ice model documentation and software user's manual version 5.1, technical report, Los Alamos National laboratory, Los Alamos NM 87545. In *Technical report LA-CC-06-012*

Large, W. G., McWilliams, J. C., & Doney, S. C. (1994). Oceanic vertical mixing: A review and a model with a nonlocal boundary layer parameterization. *Reviews of Geophysics*, *32*(4), 363–403. https://doi.org/10.1029/94RG01872

Li, Q., Webb, A., Fox-Kemper, B., Craig, A., Danabasoglu, G., Large, W. G., & Vertenstein, M. (2016). Langmuir mixing effects on global climate: WAVEWATCH III in CESM. *Ocean Modelling*, *103*, 145–160. https://doi.org/10.1016/j.ocemod.2015.07.020

Losch, M., Menemenlis, D., Campin, J. M., Heimbach, P., & Hill, C. (2010). On the formulation of sea-ice models. Part 1: Effects of different solver implementations and parameterizations. *Ocean Modelling*, *33*(1–2), 129–144. https://doi.org/10.1016/j.ocemod.2009.12.008